ROYAL INSTITUTE
OF TECHNOLOGY

Fracture toughness properties of duplex stainless steels

Henrik Sieurin

Doctoral Thesis

Department of Materials Science and Engineering
Royal Institute of Technology
SE-100 44 Stockholm, Sweden
ISBN 91-7178-354-7
ISRN KTH/MSE--06/38--SE+MAT/AVH

Stockholm 2006

ISBN 91-7178-354-7
ISRN KTH/MSE--06/38--SE+MAT/AVH

Akademisk avhandling som med tillstånd av Kungliga Tekniska Högskolan i Stockholm framlägges till offentlig granskning för avläggande av teknisk doktorsexamen onsdagen den 24 maj 2006 kl 13.30 i kollegiesalen F3, Lindstedtsv. 26, Kungliga Tekniska Högskolan, Stockholm.

Scientific thesis for the degree of Doctorate of Engineering.

Fracture toughness properties of duplex stainless steels

Henrik Sieurin
Materials Science and Engineering, Royal Institute of Technology,
Brinellv. 23, S-100 44 Stockholm, Sweden

Abstract

Good toughness properties in base and weld material enable the use of duplex stainless steels (DSS) in critical applications. DSS offer high strength compared to common austenitic stainless steels. The high strength can be utilized to reduce the wall thickness and accordingly accomplish reduction of cost, welding time and transportation weight, contributing to ecological and energy savings. Although DSS have been used successfully in many applications the last decades, the full utilisation in pressure vessels has been restricted due to conservative design rules. The consequences of failure in a pressure vessel are often very severe and it is accordingly important to verify a high ductility and fracture toughness.

In this study fracture toughness data has been generated that has been used to analyse the brittle failure model in the European pressure vessel code EN 13445. The evaluation of the results has been made successfully by the master curve analysis, previously applied to ferritic steels. The master curve analysis includes calculation of a reference temperature, which can be correlated to an impact toughness transition temperature. A correlation between fracture and impact toughness results is necessary for a practically applicable design code. The heat distribution and austenite reformation have been modelled to verify satisfactory toughness properties in the heat affected zone. A similar model was used to evaluate the nucleation and diffusional growth of sigma phase during isothermal heat treatment or continuous cooling.

For future stainless steel development, the availability of satisfactory correlations between composition, microstructure and mechanical properties are essential to optimize alloy design. Stainless steel data has been analysed to find approximate relations between mechanical properties and the chemical composition, grain size, ferrite content, product thickness and solution hardening size misfit parameter. The solution hardening effect was successfully predicted by the Labusch-Nabarro relation and multiple regression analyses were used to evaluate hardening equations for stainless steel.

Keywords: duplex stainless steel, fracture toughness, austenite reformation, sigma phase, material optimisation

Papers

The thesis is based on the following papers

- Sieurin H., Sandström R., Fracture toughness of a welded duplex stainless steel, Engineering Fracture Mechanics, Volume 73, Issue 4, March 2006, Pages 377-390.
- Sieurin H., Sandström R., Westin E. M., Fracture toughness of the lean duplex stainless steel LDX 2101, submitted to Metallurgical and Materials Transactions A, 2006.
- Sieurin H., Sandström R, Langenberg P., Crack detection performance and other assumptions for implementation in a model for avoidance of brittle fracture in pressure vessel steels, Proceeding of the 29th MPa Seminar, Stuttgart, Oct 9-10, 2003.
- Sieurin H., Sandström R., Austenite reformation in the heat-affected zone of duplex stainless steel 2205, Materials Science and Engineering A, Volume 418, Issues 1-2, February 2006, Pages 250-256.
- Sieurin H., Sandström R., Sigma phase precipitation in duplex stainless steel 2205, submitted to Materials Science and Engineering A, 2006.
- Sieurin H., Zander J., Sandström R., Modelling solid solution hardening in stainless steels, Materials Science and Engineering: A, Volume 415, Issues 1-2, January 2006, Pages 66-71.

Additional papers

- Sieurin H., Sandström R., Ericsson C., Toughness and other mechanical properties of the duplex stainless steel 2205, proceeding of the 29th MPA Seminar, Stuttgart, Oct 9-10, 2003.
- Ericsson C., Sandström R., Sieurin H., Lagerqvist O., Eisele U., Sciedermaier J., Ruiz R. L., Material and welding data; Properties and test results, background document 3.5, EcoPress, European research 5th framework, 2003.
- Sieurin H., Sandström R., Performance of duplex stainless steel with special reference to fracture toughness properties, Proceeding of the ESOPE, Paris, Sept 28-30, 2004.
- Sandström R., Langenberg P., Sieurin H., New brittle fracture model for the European pressure vessel standard, International Journal of Pressure Vessels and Piping, Volume 81, Issues 10-11, October-November 2004, Pages 837-845.
- Sandström R., Langenberg P., Sieurin H., Analysis of the brittle fracture avoidance model for pressure vessels in European standard, International Journal of Pressure Vessels and Piping, Volume 82, Issue 11, November 2005, Pages 872-881.

Contents

1. Introduction

The duplex stainless steel (DSS) family was introduced commercially about 70 years ago, mainly intended for the pulp and paper industry. A second generation with improved weldability, mainly due to higher additions of nitrogen, was developed in the early 80's. This was a breakthrough for the DSS. The use and fields of applications increase continuously. Traditional applications can be found in the chemical, oil and gas industries in applications such as pipelines and reaction vessels. DSS offers an alternative to the austenitic stainless steels especially at temperatures between –50 and 300°C and is suitable for structural applications. The two-phase structure of ferrite and austenite combines the beneficial effects of the phases and allows the steel to obtain high strength (ferrite) and toughness (austenite) even at low temperatures. The high strength makes it possible to use thinner dimensions and accomplish weight savings. Furthermore, the material offers good resistance to localized corrosion, due to high Cr, Mo and N additions, and stress corrosion cracking, due to the ferrite content [1]. Other advantages of DSS are satisfactory fatigue properties [2, 3], modest thermal expansion and modest cost due to low nickel content [4].

The phase balance in DSS obtained by careful heat treatment is crucial for the mechanical properties. DSS solidifies ferritically and a moderate cooling rate during welding and production processes promotes a favourable phase proportion. Long holding times at temperatures between 300-1000 °C and very slow cooling rates should be avoided due to precipitation of brittle intermetallic phases, such as σ and χ [5-11]. The ferritic solidification promotes resistance to solidification cracking [12]. DSS products are obtained by several different processes such as casting, forging, extrusion and rolling. Welding of DSS can be performed successfully with most of the usual welding methods [1, 13-14]. The microstructure and mechanical properties strongly depend on the specific process. The material is designed to allow welding without post weld heat treatment. A significant anisotropy is present in commercial sheet and tube materials, causing a directionality of the mechanical properties [15, 16]. The anisotropy tends to increase with the amount of rolling deformation. DSS can be produced both by hot and cold deformation, although the main product form is hot rolled plates [17]. The fracture toughness is good [18, 19] even after significant cold deformation [20, 21].

Carbon steels have traditionally been used for construction purposes due to long experience, low cost, a large variety of strength classes and applicable design rules [22]. On the other hand, there have been reservations against full utilisation of duplex stainless steels based on

lack of knowledge and experience. Pressure vessels have been produced in DSS for approximately two decades but there is a large potential for an increased use in the future. The high strength makes it possible to produce pressure vessels with a reduced wall thickness and hence to make ecology and financing savings. Brittle failure is of major concern and it is accordingly important to assess material requirements to minimize the risk of failure. Empirical rules for design against brittle failure have been available in the national pressure vessel codes for an extended period of time, unfortunately with a large discrepancy between existing codes. The first scientifically based design rules were developed by Sanz [23] and were used to establish a French national code. A Swedish national code was developed in the 80‘s based on work by Sandström [24] and was later proposed and accepted for the new European pressure vessel code, EN 13445 [25]. This model makes it possible to predict the influence of component thickness, minimum design temperature, material strength, impact toughness and post weld heat treatment. Further developments have been made in the 90‘s such as the master curve concept by Wallin [26], large extensive studies of toughness related effects such as residual stresses [27] and the influence of elasto-plastic effects [28]. The DSSs are in EN 13445 evaluated according to design criteria for ferritic steels. In order to use the more favourable austenitic design criteria, satisfactory ductility and prevention of brittle failure at sub-zero temperatures have to be assumed and verified experimentally. The fracture toughness describes the ability of a material containing a crack to resist fracture. Well documented fracture toughness is of great importance for design applications. New applications for DSS arise continuously and new grades with modified chemistry are developed, requiring great knowledge of heat treatment, welding and alloying.

2. Aim of work

The aim of the work has been to study fracture toughness related properties of duplex stainless steels. The reference material for most of the work has been a 22Cr-5Ni-3Mo-0.17N DSS. The PhD work was initiated in 2000 within a EU project financed by the 5th framework, EcoPress [29], concerning high strength steels for pressure vessel applications. An objective of this project was to find acceptance for high strength steels in the revision of the European pressure vessel code EN 13445 [25]. The Swedish part of the project focused on duplex stainless steel, including fracture toughness testing of base and weld material. When EcoPress was finished in 2003, the PhD studies continued within the MATOP [30] research project. The purpose of the MATOP program is to develop necessary tools and collect and assess

required data to establish materials optimisation as a powerful tool in material and process development. The issues discussed in the thesis can be summarized as:

- Fracture toughness testing and master curve analysis of DSS base and weld material.
- Analysis and revision of the model in the European pressure vessel code EN 13445 for prevention of brittle failure taking recent developments in fracture mechanics into account. The new model has been tested against new fracture mechanic data to confirm the validity of the model for DSS.
- Modelling of the heat distribution, cooling rate and austenite reformation to verify satisfactory balance between ferrite and austenite in the heat affected zone (HAZ). A similar model based on nucleation and diffusional growth has been applied to predict the sigma precipitation due to aging or continuous cooling.
- Establishment of models by regression analyses in order to predict the mechanical properties from chemical composition, solution hardening misfit parameters, grain size, ferrite content and product thickness.

3. Duplex stainless steels

Stainless steels can be divided into the ferritic, austenitic, martensitic and duplex family. The duplex family offers a good combination of economy, weldability and toughness and are often selected where both strength and corrosion properties are crucial [31]. DSSs are more technically demanding than the standard austenitic stainless steel grades such as type 304 and 316, but offers superior corrosion resistance in various aggressive environments. It is important to avoid secondary phases and to maintain the favourable balance of ferrite and austenite during fabrication and welding. The applications have mainly been in components with corrosion requirements, but there is a potential for increased use in structural applications due to the good mechanical properties. The development of duplex grades today involves both higher alloyed steels for improved corrosion resistance [32, 33] and lower alloyed steels for construction purposes and reduced cost [22]. The typical chemical composition of four DSS grades is shown in Table 1 [22, 34].

Table 1. Typical chemical composition (wt-%) of important duplex grades.

	Cr	Ni	Mo	Mn	N
2304 [34]	21.5-24.5	3.0-5.5	0.05-0.6	2.5	0.05-0.2
LDX 2101 [22]	21.5	1.5	0.3	5	0.22
2205 [34]	22.0-23.0	4.5-6.5	3.0-3.5	2	0.14-0.20
2507 [34]	24.0-26.0	6.0-8.0	3.0-5.0	1.2	0.24-0.32

The characteristics of some duplex grades:

- 2304 (EN 1.4362, UNS S32304) is a relatively low alloyed (lean) DSS with similar corrosion resistance as the standard austenitic stainless steels. However, it offers higher strength and better stress corrosion resistance [31].
- LDX 2101 (EN 1.4162, UNS S32101) is a recently developed lean DSS with low additions of nickel in order to reduce and stabilise the cost. The low content of nickel is compensated by an increased amount of manganese and nitrogen to assure a high austenite fraction. The strength of this material is comparable with DSS 2205 and the corrosion properties are at least better than for austenitic 304 [22].
- The most common duplex grade today is 2205 (EN 1.4462, UNS S32205) [22], which is a medium alloyed DSS with better corrosion properties compared to the standard austenitic stainless steels. The fabrication, weldability and economical properties are also satisfactory.
- 2507 (EN 1.4410, UNS S32750) is a high alloyed DSS, usually called super duplex, which offers high strength and resistance to corrosion in extremely aggressive environments [34]. However, thermal treatments of super duplex stainless steel must be performed carefully since the high chromium and molybdenum contents involve rapid formation of secondary phases at high temperatures.
- Sandvik SAFUREX (UNS S32906) is a modern super duplex stainless steel developed to withstand the corrosion environments present in the stamicarbon urea process [35]. This alloy has high chromium and nitrogen content and moderate amounts of molybdenum [36]. This composition provides a unique combination of high strength, excellent corrosion resistance and good weldability.

The Schaeffler-DeLong diagram [37] can be used to predict the microstructure from the chemical composition in stainless steel weldments or castings, Fig. 1 [38]. The alloying

elements stabilizing the ferrite are called Cr-equivalents and the elements stabilizing the austenite are called Ni-equivalents [37]:

$$\text{Cr}-\text{equivalent} = Cr + Mo + 1.5Si + 0.5Nb \quad [\text{wt\%}] \tag{1}$$

$$\text{Ni}-\text{equivalent} = Ni + 30(C + N) + 0.5Mn \quad [\text{wt\%}] \tag{2}$$

The ferrite content is given as the ferrite number, FN, which can be estimated by the following expressions [39].

$$\text{FN} = 3.34Cr_{eq} - 2.46Ni_{eq} - 28.6 \qquad \text{FN} < 6 \tag{3}$$

$$\text{FN} = 4.44Cr_{eq} - 3.39Ni_{eq} - 38.4 \qquad 6 \le \text{FN} \le 12 \tag{4}$$

$$\text{FN} = 4.06Cr_{eq} - 3.23Ni_{eq} - 32.2 \qquad \text{FN} \ge 12 \tag{5}$$

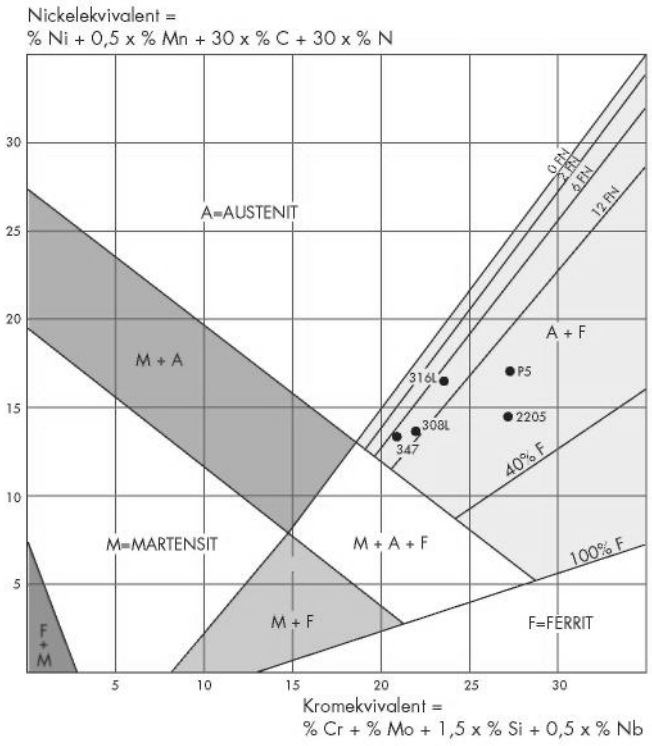

Fig. 1. Schaeffler-DeLong diagram showing the effect of the Cr- and Ni-equivalents on the phase structure [38].

The microstructure in DSS is usually composed of approximately equal amounts of austenite and ferrite. The austenite is placed as laths in a ferrite matrix. The austenite ratio can be increased to about 55-60 % in order to improve the toughness properties and maintain a sufficient austenite ratio in the HAZ [17]. The desired microstructure is usually obtained by hot working, followed by solution annealing and quenching to ambient temperature [17]. Hot working is usually performed in the temperature range 1000-1200 °C [5]. A typical base

material microstructure with a fine lamellar grain size is shown in Fig. 2a. The coarser structure of a submerged arc weld is shown in Fig. 2b.

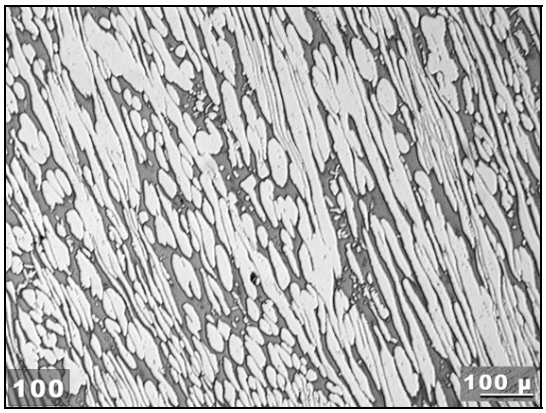

Fig. 2a. Light optical micrograph of base material, 2205. The austenite fraction is approximately 60 %.

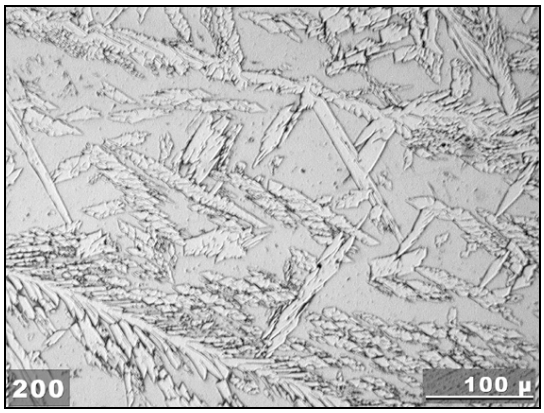

Fig. 2b. Light optical micrograph of submerged arc weld metal, 2205. The austenite fraction is approximately 45 %.

The etchant colours the ferrite matrix dark and the austenite white. In the weld metal, the austenite is reformed mainly at the grain boundaries and grows as Widmanstätten plates into the grains, see Fig. 2b.

3.1 Mechanical properties

The yield strength of DSS is 2-3 times higher than for 18Cr-10Ni austenitic stainless steels. The ferrite usually contributes to the high strength, but the strength in DSS is also higher than for pure ferritic stainless steels [31]. This can be explained by the small grain size in DSS [5], caused by mutual hindering of the growth of the ferrite and austenite grains [40], implying higher strength for the two phase structure than its constituents. It has also been shown that the austenite might be stronger than the ferrite due to interstitial solid solution hardening of nitrogen in the austenite [5]. The high yield strength in DSS is the result of [41]:

- Presence of ferrite
- Small grain size
- Formation of hard secondary austenite
- Interstitial and substitutional solution hardening

The yield and tensile strength of 2205, base and weld (SAW) material, are shown in Fig. 3 [21] as a function of temperature.

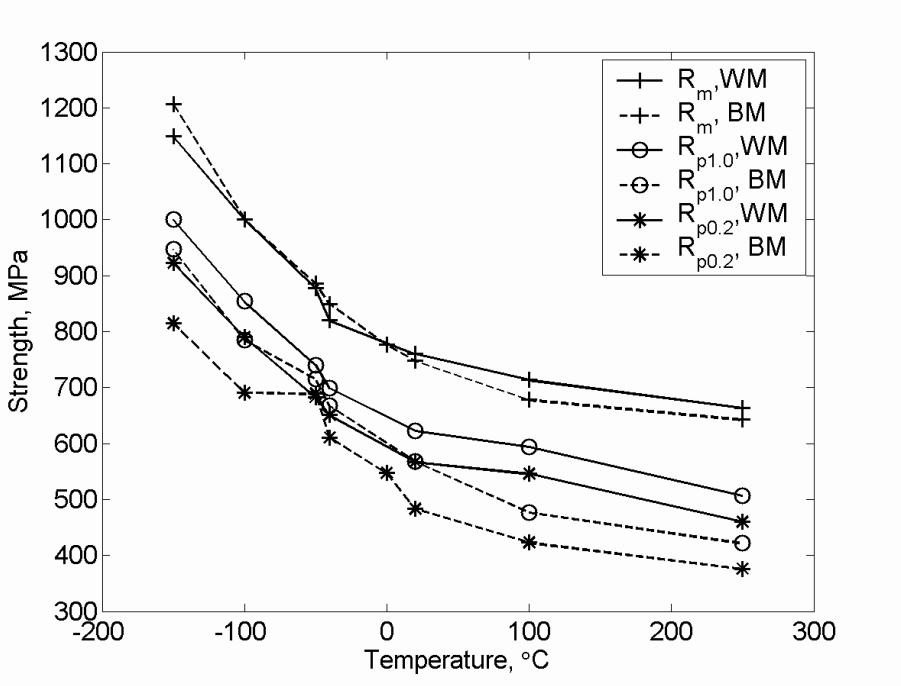

Fig. 3. Strength properties of base material (BM) and weld material (WM) in the transverse direction of 30 mm thick duplex 2205 [21]. R_m is the tensile strength while $R_{p0.2}$ and $R_{p1.0}$ are the yield strengths evaluated at 0.2 and 1.0% deformation.

The difference in tensile strength between base and weld material is small, while it is more pronounced for the yield strength. The weld material has a higher ferrite fraction compared to the base material and it has been shown that the ferrite in a DSS decrease the tensile strength and increase the yield strength [42]. Regression models describing the yield and tensile strengths of austenitic and DSS was given by Nordberg in [43].

$$\sigma_{ys0.2} = 120 + 210\sqrt{N + 0.02} + 2Mn + 2Cr + 14Mo + 10Cu + (6.15 - 0.054\delta)\delta + \left[7 + 35(N + 0.02)\right]d^{-0.5} \quad [MPa] \tag{6}$$

$$\sigma_{ys1.0} - \sigma_{ys0.2} = 40 \pm 9 \quad [MPa] \tag{7}$$

$$\sigma_m = 470 + 600(N + 0.02) + 14Mo + 1.5\delta + 8d^{-0.5} \quad [MPa] \tag{8}$$

The model correlates the yield and tensile strength with the chemical composition, ferrite content (δ) and grain size (d). New regression models have been developed, also considering product thickness and solid solution hardening [44]. The tensile strength is higher in the transverse direction compared to the longitudinal [16]. The anisotropic plastic flow properties are a result of crystallographic texture rather than a microstructure effect [2, 16]. A comparison of the mechanical properties of four duplex grades can be found in table 2.

Table 2. Minimum mechanical properties for DSSs.

Grade	$R_{p0.2}$ [MPa]	R_m [Mpa]	A_5 [%]
2304 [31]	400	600	25
LDX 2101 [45]	450	650	30
2205 [31]	450	620	25
2507 [31]	550	795	15

Both yield strength, tensile strength and hardness are improved by cold rolling, while the elongation is slightly reduced, see Fig. 4 [21].

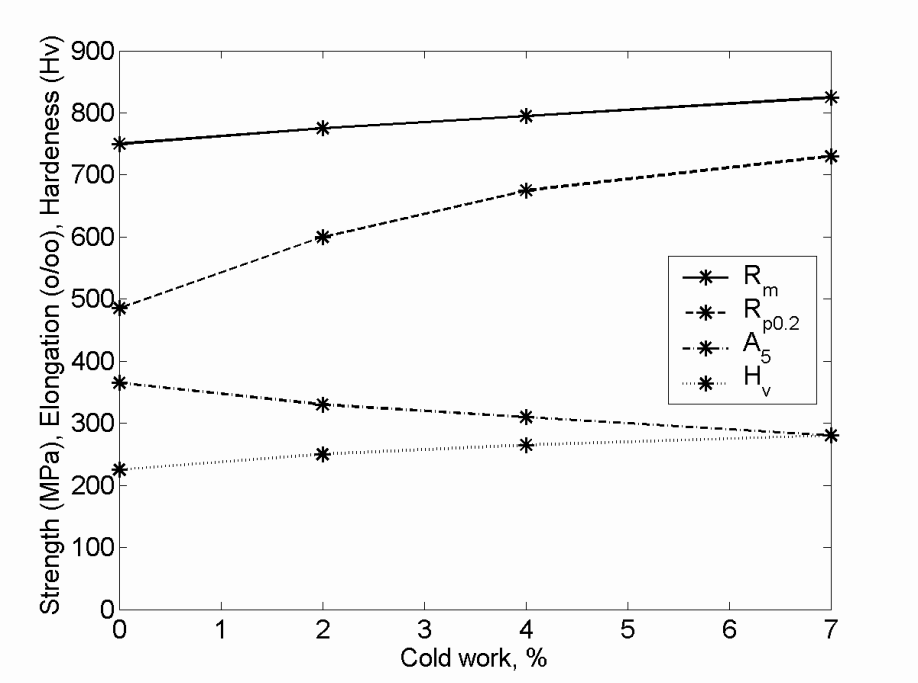

Fig. 4. The effect of cold work on the tensile strength (R_m), yield strength ($R_{p0.2}$), elongation (A_5) and hardness (H_V) [21].

The effect of cold rolling is small on the tensile strength, elongation and hardness while the increase of the yield strength is pronounced.

The modulus of elasticity for base and weld material is shown in Fig. 5 as a function of temperature [21].

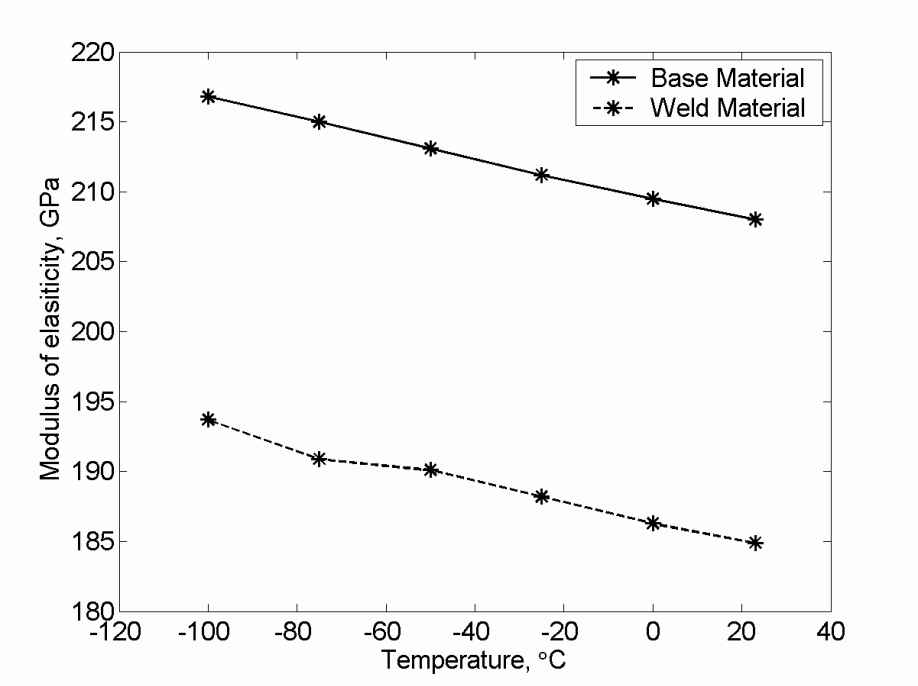

Fig. 5. Modulus of elasticity of 30 mm thick duplex 2205 base and weld material. The base material was located at quarter thickness in transverse orientation, the weld material at the surface in the longitudinal direction [21].

The modulus of elasticity decreases slightly with increasing temperature, the value of the base metal being approximately 23 GPa higher compared to the weld metal, independent of the temperature.

Biaxial testing has been performed at Luleå University of Technology on 4 mm thick cold rolled strips of duplex 2205 [21]. The load was applied by oil pressure and the bulge was measured. The tests were performed to verify the formability of DSS in fabricated and multiaxial condition. Three types of specimens were tested; plain sheet, butt welded sheet and welded nozzle. Results of the membrane tests are shown in Table 3.

Table 3. Results of membrane tests [21].

Sample	Internal pressure at failure, MPa	Bulge at failure, mm	Location of failure
Plain sheet	39.6	80.2	Crack along RD, top of membrane
Butt weld	40.1	70.1	HAZ
Welded nozzle	30.2	46.0	Weld

The bulge at failure in the plain sheet was approximately 80 mm, which corresponds to a total strain resultant of 40 % at failure. The welded nozzle had a bulge at failure of approximately 45 mm, which corresponds to a strain of 13 % at failure. According to EN 13445-4, the maximum operating strain should be less than 5 % and consequently the ductility in these

components is fully adequate. The fracture pressure in all cases was far beyond the typical pressure in a vessel.

The fatigue strength of DSS corresponds approximately to the proof stress of the material [1]. A study by Iacoviello et al [46] of solution annealed and embrittled duplex 2205 showed a clear influence of aging on the crack grow rate. The highest crack growth rates were obtained when aging at high temperatures (800°C). A difference in crack propagation mechanisms in non-aged and aged DSS was observed by Stolarz et al [47]. In non-aged materials the ferrite and the austenite are plastically deformed and short cracks can nucleate inside the grains of both phases. The cracks are arrested at the phase boundaries before they propagate through the neighbouring grains. In the aged material the ferrite becomes very hard and the plasticity is concentrated to the austenite. Stress concentrations are created in the brittle ferrite grains and promote brittle fracture locally in the ferrite. An improved low cycle fatigue resistance can be obtained by increasing the nitrogen content in DSS [2]. Nitrogen is an austenite stabilizer and an increased austenite content is beneficial for controlling the distribution of the fatigue damage and the cyclic softening. The positive influence of increasing the austenite fraction in DSS by enhanced nitrogen content was shown by Vogt et al [48]. It was suggested that a relatively high volume fraction of austenite, i.e. increasing the average size of the austenite domains, will prevent the cracks in the brittle ferrite matrix to propagate through overlapped plastic austenitic areas. Alloying with 0.4 % nitrogen, resulting in an alloy composed of 70% austenite and 30% ferrite, offered beneficial fatigue performance. High cycle fatigue (HCF) of a bar and a plate made of duplex 2205 was studied by Mateo et al [3]. It was shown that the ferrite was the dominating phase carrying the plastic deformation at high stress levels, close to and above the fatigue limit. It was established that the fatigue properties were mainly controlled by the ferrite matrix for HCF and that the fatigue resistance was anisotropic, with the best fatigue resistance perpendicular to the rolling direction.

The toughness properties in DSS are mainly governed by the austenite phase and are satisfactory if the material is properly treated. However, aging in the temperature range 600-950°C might rapidly decrease the toughness, with the most severe effect at around 900°C. The reduced toughness is due to formation of brittle σ and χ-phase. It was shown by Thorvaldsson et al [6] how a marked transition from ductile to brittle behaviour occurred for ageing times up to 1 hour at 850°C. The impact toughness decreased from over 290 to 4 J and was after 1 hour relatively constant. Another decrease of the toughness is caused by the 475°C embrittlement, which causes decomposition of ferrite to α and α'- phase. A high dislocation

density due to deformation enhances the α precipitation [16]. Other factors reducing the toughness are high ferrite content and high levels of oxygen and hydrogen [49]. A maximum service temperature of 300°C is often suggested [4]. The toughness is higher in the transverse direction compared to the longitudinal since a crack growing in the transverse direction has to pass through the phase boundaries of the lamellar structure. The transition from ductile to brittle fracture shifts to higher temperatures with increasing specimen thickness. Welding if not properly performed can also decrease the toughness properties due to decomposition of the original two-phase structure and with precipitation of secondary phases. Different duplex stainless steel grades offer satisfactory impact toughness down to temperatures as low as -50 to -100°C [4]. Impact toughness testing has been performed on 30 and 50 mm thick duplex 2205, both base and weld material [21]. The transition temperatures T_{27J} and T_{40J}, which are the temperatures corresponding to an impact energy of 27 and 40 J respectively, are given in Table 4.

Table 4. Impact toughness of duplex 2205 base material, weld material and fusion zone [21].

Thickness, mm	Condition	Direction	Position	T_{27J}, °C	T_{40J}, °C
30	Base material	T-L	t/4	-133	-115
30		T-S	t/4	-143	-122
50		T-L	t/4	-114	-101
30	Weld material	T-L	t/4	-63	-54
30		T-S	t/4	-	-44
50		T-L	Surface	-98	-84
50		T-L	t/2	-69	-57
30	Fusion zone	T-L	-	-	-80
30		T-L	-	-86	-77

Notches were machined with transverse-longitudinal (T-L) and transverse-short (T-S) orientation (the first symbol (T) describes the plane and the second symbol (L, S) describes the propagation direction of the notch). It is shown that the T-L direction in the base material has a slightly lower toughness compared to the T-S direction. However, all the base material results are satisfactory with transition temperatures below -100°C. The thicker 50 mm specimens give the lowest transition temperatures. The base material impact toughness results from specimens tested at quarter thickness are shown in Fig. 6 [21].

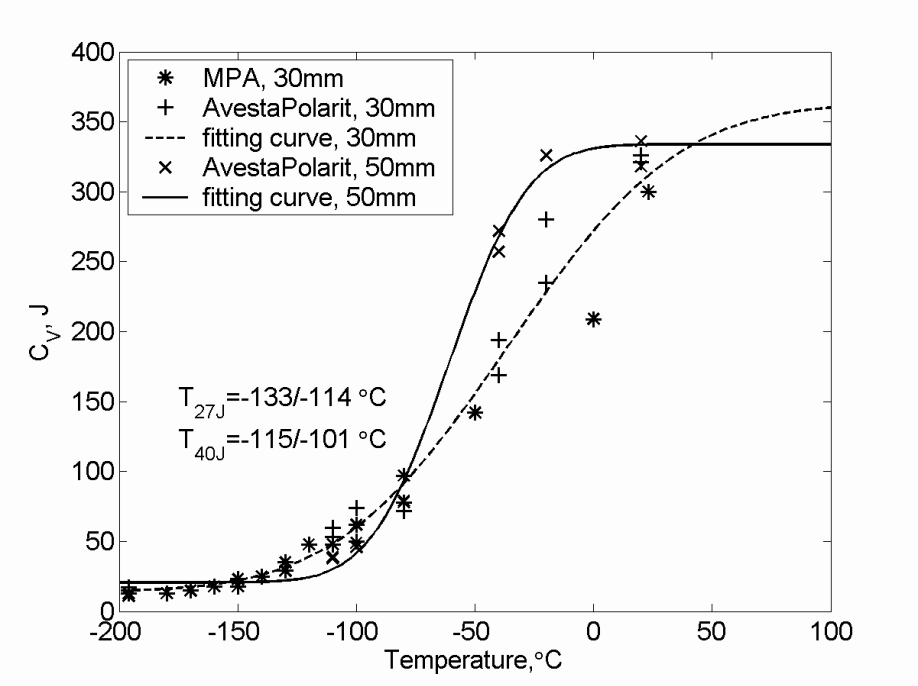

Fig. 6. Impact toughness (C_v) for 30 and 50 mm thick duplex 2205 base material [21].

It can be seen that the 50 mm material has the steepest transition temperature curve. The weld material gave transition temperatures approximately 60-80°C higher compared to the base material. However, the transition temperatures were still well below ordinary service temperatures. The T-S direction gave a slightly higher transition temperature compared to the T-L direction. The 50 mm specimens were tested at half thickness and at the surface. The surface specimens had the highest toughness. The weld material results from specimens tested at quarter thickness can be found in Fig. 7 [21].

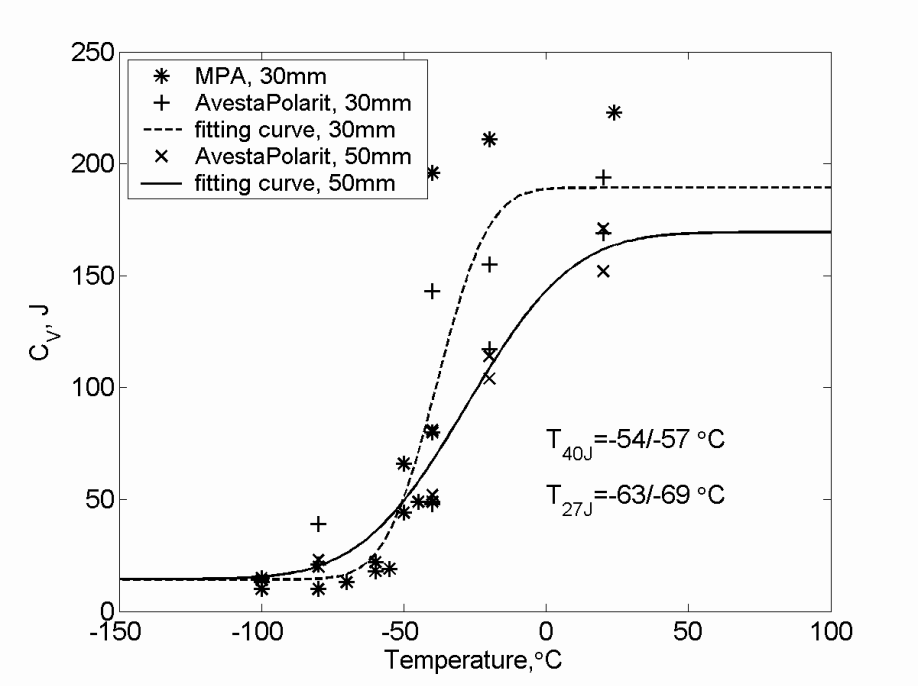

Fig. 7. Impact toughness (C_v) for 30 and 50 mm thick duplex 2205 weld material [21].

The 30 mm material gave a slightly higher transition temperature and had a steeper transition temperature curve compared to the 50 mm material, in contrast to the base material. Fracture surfaces of 50 mm impact toughness specimens, tested at room temperature and at -100°C can be found in Fig. 8 [21].

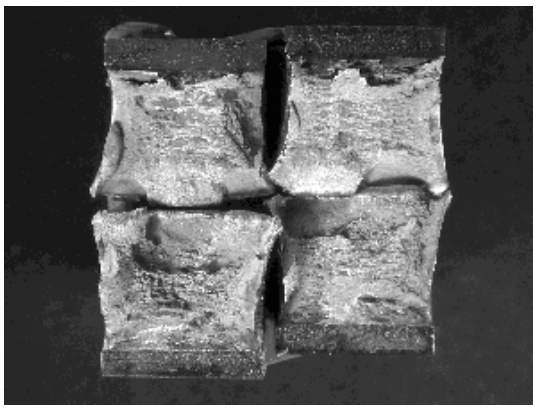

Fig. 8a. Charpy V weld material specimen from a plate of 50 mm thickness, tested at room temperature. The notches were oriented T-L and the impact toughness were 152 and 171 J, respectively.

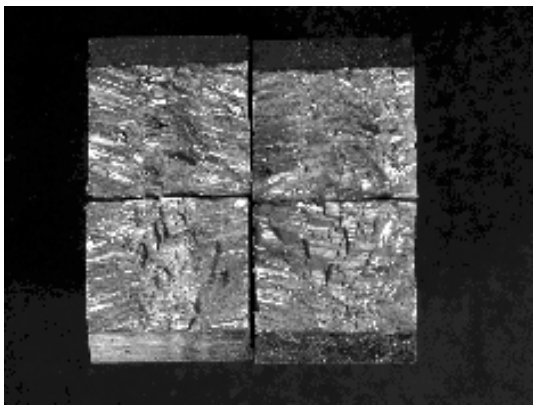

Fig. 8b. Charpy V weld material specimens from a plate of 50 mm thickness, tested at -100°C. The notches were oriented T-L and the impact toughness were 14 and 15 J, respectively.

The specimens tested at room temperature give high impact toughness and the fracture surfaces have a fibrous character with shear fracture along the surfaces. The specimens tested at -100°C have cleavage-like modes of fracture with flat reflective surfaces.

Cold deformation might be acceptable since the toughness remains high. A comparison of the impact toughness for 0, 4 and 7 % cold work is shown in Fig. 9 [21].

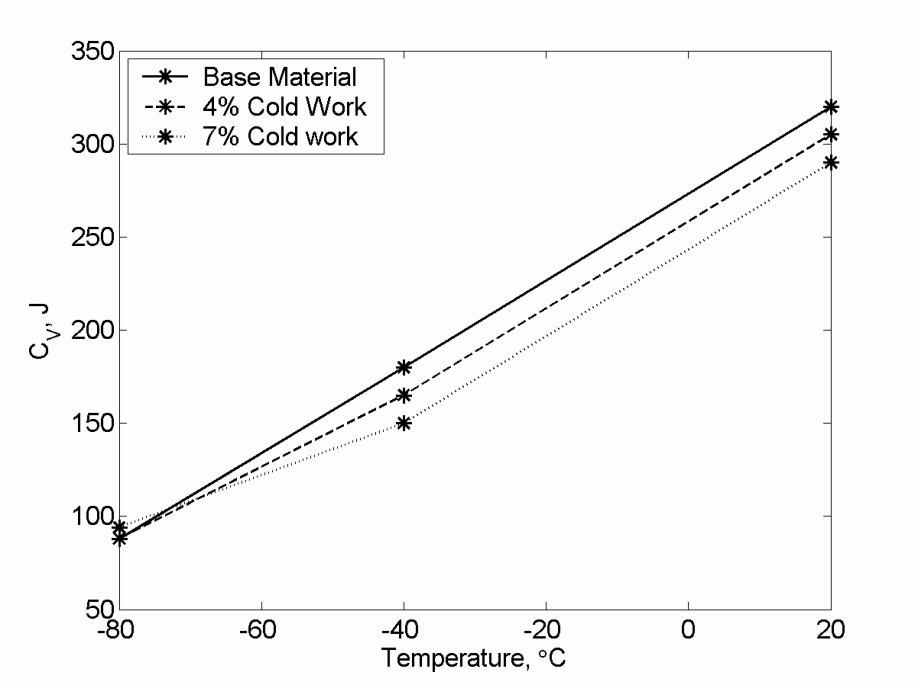

Fig. 9. Influence of cold work on the impact toughness.

The influence from cold deformation is small and seems to be negligible at low temperatures. It was also shown that minor amount of deformation was sufficient to significantly increase the yield strength, see Fig 4. The same conclusion was drawn by Fourlaris et al [50].

3.2 Welding

DSSs have good weldability and most of the usual welding methods can be used such as submerged arc welding (SAW), shielded metal arc welding (SMAW), gas tungsten arc welding (GTAW) and gas metal arc welding (GMAW) [14, 51]. A typical welding consumable for DSS usually contains an increased amount of nickel in order to stabilize the austenite and to avoid precipitation of nitrides and secondary austenite [12]. The tensile properties of DSS weldments are generally acceptable, while the toughness properties are strongly dependent of welding procedure, filler material and microstructure. A comparison of impact toughness data for different welding methods in the weld metal and the fusion zone of duplex 2205 is shown in Fig. 10 [21].

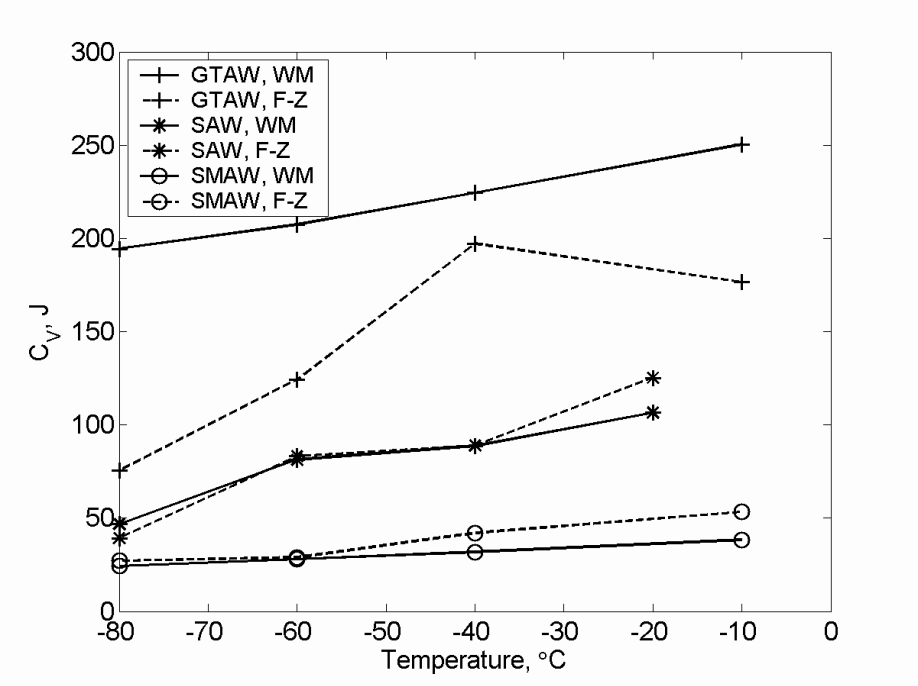

Fig. 10. Impact toughness versus temperature for duplex 2205 weld metal and fusion zone in gas tungsten arc welding (GTAW), submerged arc welding (SAW) and shielded metal arc welding (SMAW) [21].

The GTAW method generates the highest impact toughness, followed by SAW and SMAW. The lower toughness in SAW and SMAW can be explained by higher oxide levels. However, GTAW welding is best suited for thin materials, from about 0.5 mm to 3 mm [52]. The understanding of the changes in microstructure during welding is essential to produce sound weldments. The ferritic solidification, followed by the solid state ferrite-austenite transformation during welding and heat treatment can be illustrated in a pseudo binary diagram, see Fig. 11 [53].

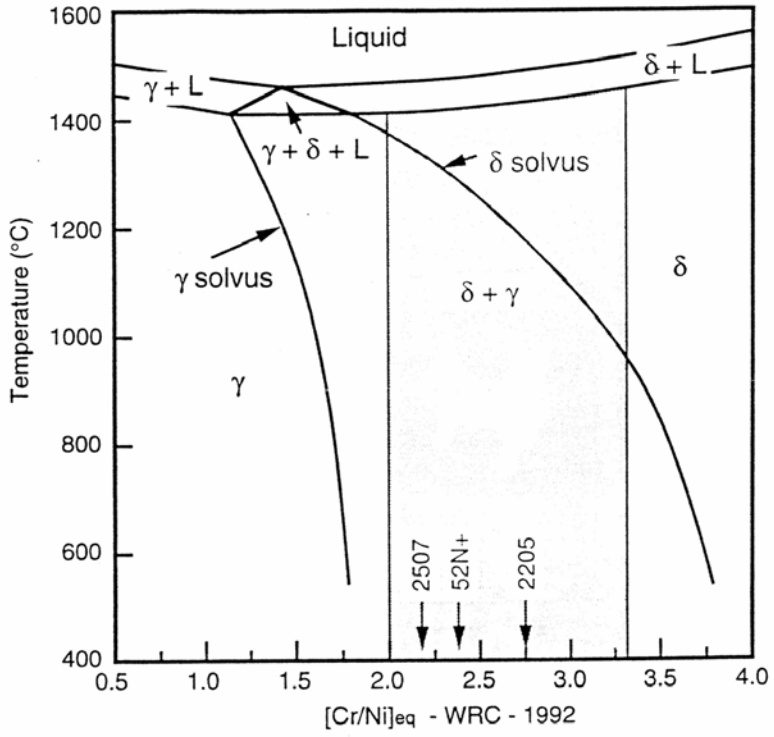

Fig. 11. Pseudo binary diagram plotted using WRC-1992 equivalent relationships [53].

The grade 2205 has a larger temperature range between the solidus and ferrite solvus temperature, causing a more ferritic HAZ than the super duplex grade 2507. A long holding time above the ferrite solvus will give larger grain sizes and higher ferrite fraction. The melting and solidification associated with fusion welding change the favourable base material microstructure and produce coarse ferrite grains with intergranular and intragranular austenite. Moreover, the balanced fraction of ferrite and austenite might be destroyed. This balance is part of the reason for the attractive mechanical and corrosion properties but can be retained by proper welding parameters and a suitable weld filler material. In general, the volume fraction of ferrite is much higher compared to austenite in the weld metal and the HAZ, but a sufficiently high austenite fraction can be achieved by high heat input and slow cooling rate. However, these conditions also produce a coarse microstructure in the weld, a wide HAZ and precipitation of brittle intermetallic phases. On the other hand, the rapid cooling rate in some weld processes causes a surplus of brittle ferrite. High super saturation of nitrogen in the ferrite compared to the austenite can cause precipitation of nitrides in the ferrite [54, 55]. Precipitation of Cr_2N can occur in the HAZ during fast cooling, e.g. due to low heat input. Enhanced Cr_2N precipitation has been found in a simulated HAZ at cooling times between

1200 and 800°C of 2-20 seconds [55]. The presence of Cr_2N can reduce the pitting corrosion resistance. To avoid this effect a lower heat input limit of 0.46 kJ/mm has been suggested for GTAW [56]. The phase balance can also be retained by choosing a proper weld filler material, often with an enhanced amount of nickel. The austenite reformation has been found to be controlled by redistribution of nitrogen instead of diffusion of the slower diffusing metallic elements (para-equilibrium) [57]. Nitrogen depletion can be avoided by using a nitrogen containing shielding gas. Multipass welding can cause diffusional transformation of ferrite to austenite in reheated areas of 900-1050°C, as well as precipitation of intermetallic phases if the peak temperature is 700-800°C and the cooling rate is slow [58]. The ferritic solidification mode of DSS involves high solubility of sulphur and phosphorus impurities and small thermal expansion, which opposes solidification cracking that can occur in austenitic solidified stainless steels during multipass welding [12, 56]. The secondary austenite precipitated below 900°C has lower contents of N, Cr and Mo compared to the primary high temperature austenite [59].

It was shown by Muthupandi et al [60] that the chemical composition has a great influence on the phase balance in addition to that of the cooling rate. It was also shown that electron beam welding (EBW), suitable for welding thick components, can be applied to DSS. An acceptable phase balance can be obtained provided nickel enrichment of the weld can be made, for example by using preplaced nickel foils. Satisfactory impact toughness results were achieved on as-welded and solution-treated specimens at room temperature and at -40°C. The solution-treated specimens had a significantly higher toughness, although the ferrite content did not differ much.

Oxygen has negligible solubility in steel and it is important to choose a flux giving low oxygen content to achieve a high toughness [49]. Submerged arc welding (SAW) has been used successfully for welding DSS for an extended period of time. The favourable weldability of SAW was reassessed by McPherson et al [13], who also pointed out the possibility of an increased use in the future for SAW of DSS 2205. Acceptable material and corrosion properties were also achieved by laser welding of duplex 2205, though the authors claimed that further work is required. Submerged arc welding of DSS to carbon steel might cause problems due to heavy and/or uneven dilution and precipitation of hard zones in the weld metal [20]. This problem was reduced by minimising the dilute zone by using a proper V edge preparation. The favourable microstructure of DSS can be maintained by friction stir welding (FSW) [61], which is a solid-state welding method. The microstructure in the weldment is

refined through dynamic recrystallisation and the yield and tensile strength of the weldment is roughly the same as for the base material. FSW was developed in the early 90's and has been restricted to lower melting temperature materials, such as aluminium. Few papers have been published so far dealing with FSW of DSS.

Despite the anisotropy and coarse structure of DSS weldments, non destructive testing methods such as specialized ultrasonic techniques can be used for weld inspection [62].

3.3 Phase transformations

The duplex microstructure is most often in a metastable state, preserved by fast cooling after solution heat treatment at a temperature above 1030 °C [63]. Heat treatment and cooling after solution treatment or welding should be properly handled in order to avoid decomposition of the original microstructure and precipitation of secondary phases, often deteriorating the corrosion and toughness properties. The γ-α phase regime for solution treatment and the presence of intermetallic phases at lower temperatures can be found in the binary phase diagram of Fe-Cr in Fig. 12.

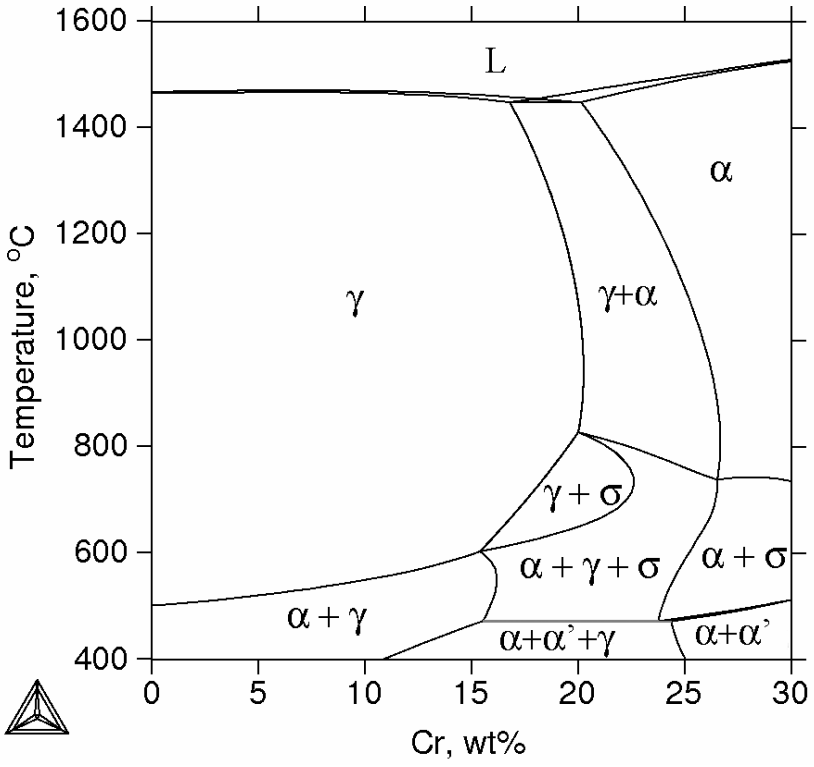

Fig. 12. Binary phase diagram of Fe-Cr system [64].

3.3.1 Austenite reformation

The performance of DSS can be significantly affected by the balance between ferrite and austenite. DSS solidifies as ferrite which on further cooling transforms partially to austenite. During cooling, austenite is first precipitated at the grain boundaries, followed by Widmanstätten plates and finally as intragranular precipitates [65-67]. A small grain size enhances the austenite reformation due to increased grain boundary area [68]. The grain boundary and Widmannstätten precipitation requires a relatively smaller driving force and can consequently occur at higher temperatures, with less undercooling [69]. Austenite stabilizers used in DSS are nickel, manganese and nitrogen. Nickel and nitrogen raise the start temperature for austenite formation [57] and nitrogen promotes the formation of Widmanstätten plates [69]. For a given chemical composition, the reformed austenite fraction depends mainly on the cooling rate, inclusion content and grain size [70]. Inclusions are potential nucleation sites for austenite.

3.3.2 Intermetallic precipitation

Various secondary phases might precipitate in DSS due to incorrect heat treatment in the temperature range 300-1000 °C, i.e. σ, χ, Cr_2N and $M_{23}C_6$ [4-6]. The formation of these phases has a detrimental effect on corrosion resistance and toughness. The precipitation is usually caused by decomposition of the ferrite phase, which contains large amounts of Cr and Mo, has low solubility of N and C and exhibits fast diffusion within the BCC crystal structure. The diffusion rates in austenite are significantly lower than in ferrite. Solution treatment of DSS 2205 in the temperature range of 1020-1080 °C dissolves the secondary phases without affecting the ferrite-austenite phase balance [72]. The equilibrium chemical composition of ferrite (δ), austenite (γ), sigma (σ) and chi (χ) in DSS 2205 at 650 °C can be found in table 5. The compositions were given by Thermo-Calc [64].

Table 5. Chemical composition of 2205 and present phases at 650 °C during equilibrium [64].

Phase	Cr	Ni	Mo	Mn
2205	21.46	5.50	2.98	1.46
δ	17.26	2.82	0.91	0.50
γ	14.17	8.37	0.76	2.08
σ	38.76	2.57	5.50	1.57
χ	24.37	2.58	13.13	-

The crystallographic characteristics of some phases that can precipitate in DSS can be found in table 6.

Table 6. Lattice types and lattice parameters of DSS phases [65].

	δ	γ	σ	χ	$M_{23}C_6$	R
Lattice type	BCC	FCC	Tetragonal	BCC	FCC	Trigonal
Lattice parameter (nm)	a=0.2866	a=0.3539	a=0.88 c=0.4583	a=0.8920	a=1.0645	a=1.0903 c=1.9342

Sigma (σ) phase is usually the most important of the secondary phases since it can be present at the highest volume fractions and clearly devastates the toughness and corrosion properties [71, 73]. The precipitation occurs between 600 and 1000 °C [5] and often starts at triple junctions or grain boundaries and grows into the ferrite. The formation can be suppressed by a high solution temperature, due to dilution of σ formation elements in the ferrite [71, 72]. Super duplex stainless steels with high additions of Cr and Mo are most prone to sigma precipitation, since these elements are enriched in sigma. A study of DSS 2205 indicated the following stochiometry, independent of temperature:
$(Fe_{0.95}Ni_{0.04}Mn_{0.01})_{0.61}(Cr_{0.88}Mo_{0.09}Si_{0.03})_{0.39}$ [65].

Chi (χ) phase precipitates in the temperature range 700-900 °C [5] and has a similar effect on the material as σ, but occurs mainly at somewhat lower temperatures, where the diffusion is slower [74, 75]. Moreover, χ needs large amount of Mo to form [76]. This can explain why the precipitated volume fraction of χ is significantly lower compared to σ in commercial DSS. χ phase is more unstable than σ phase and might eventually transform into σ phase during aging [77]. The stochiometry of chi phase is $Fe_{36}Cr_{12}Mo_{10}$[63].

Cr_2N nitrides precipitate between 700 and 900 °C during rapid cooling or isothermal heat treatment. Slow cooling rates reduce the amount of Cr_2N due to increasing austenite formation, where nitrogen can dissolve [55]. The precipitation decreases the pitting corrosion resistance due to depletion of Cr and N [54, 55, 78].

$M_{23}C_6$ carbides have high mobility and can form prior to other phases at the grain boundaries, acting as nucleation sites for later formed secondary austenite and σ [65, 79]. Modern duplex stainless steels have low contents of C and carbide precipitation is unlikely to occur [5].

R phase is Mo rich and can be found between 550-650 °C, uniformly distributed throughout the ferrite grains [65]. The corrosion and toughness properties are reduced due to R phase precipitation.

α and α´ phase form in the temperature range 300-500 °C, often referred to as the 475 °C embrittlement [75]. The formation of Fe rich α phase and Cr rich α´ phase is a consequence of spinodal decomposition of ferrite [5, 75, 80]. The time for α´ formation is very long, 10 h for 2507 and 20 h for 2205 [75].

Secondary austenite formed during welding and heat treatment will have a different composition compared to primary austenite, since the equilibrium composition is a function of temperature. The decomposition of the supersaturated ferrite into secondary austenite can take place by an eutectoid reaction ($\delta \rightarrow \sigma + \gamma$), as Widmannstätten precipitates or by a martensitic process [5]. The secondary austenite has a higher Ni content and a lower Cr and Mo content compared to the primary austenite, causing lower pitting corrosion resistance.

4. Development of the understanding of fracture toughness for ferritic steels

The risk for brittle failure in a component increases with thickness, presence of defects such as in welds and decreasing temperature. The linear elastic stress intensity factor (K_I) in front of a crack can be expressed as

$$K_I = f\sigma\sqrt{\pi a} \tag{9}$$

where f is a geometrical factor, σ is the stress in front of a sharp crack and a is the crack depth of an elliptical surface crack. When the stress intensity factor reaches a critical value the specimen will break. This critical value, describing resistance of a component against flaws, is called the fracture toughness (K_C). In thick specimens with plane strain behaviour the fracture toughness is independent of material thickness and is designated K_{IC}. Traditional linear elastic methods [81-83] to evaluate K_{IC} require very large specimens and low temperatures for tough steels. For common structural steels, including DSS with a relatively high toughness and plane stress behaviour, plastic deformation takes place in front of the crack tip. For these materials the J-integral can be calculated [84], which describes the energy release rate for non-linear elastic materials. This method of determining toughness is based on the amount of energy required to initiate and propagate a crack. To determine the J-integral the specimen is loaded while the crack mouth opening displacement (CMOD) is measured continuously. The area beneath the load-CMOD curve gives the amount of energy required for fracture. Analysis of the results enables a J factor to be calculated as a measure of fracture toughness. The critical J-value (J_c) is evaluated where a discontinuity in the load-displacement record can be observed or a maximum force plateau is reached. The J_c value can be used to calculate the

critical elasto-plastic stress intensity factor (K_{JC}), characterising failure after more or less extended ductile crack growth.

$$K_{JC} = \sqrt{\frac{J_c \cdot E}{\left(1-\nu^2\right)}} \tag{10}$$

The temperature is one important factor controlling a fracture to be brittle or ductile. The range between fully brittle and ductile fracture is called the transition range, see Fig. 13.

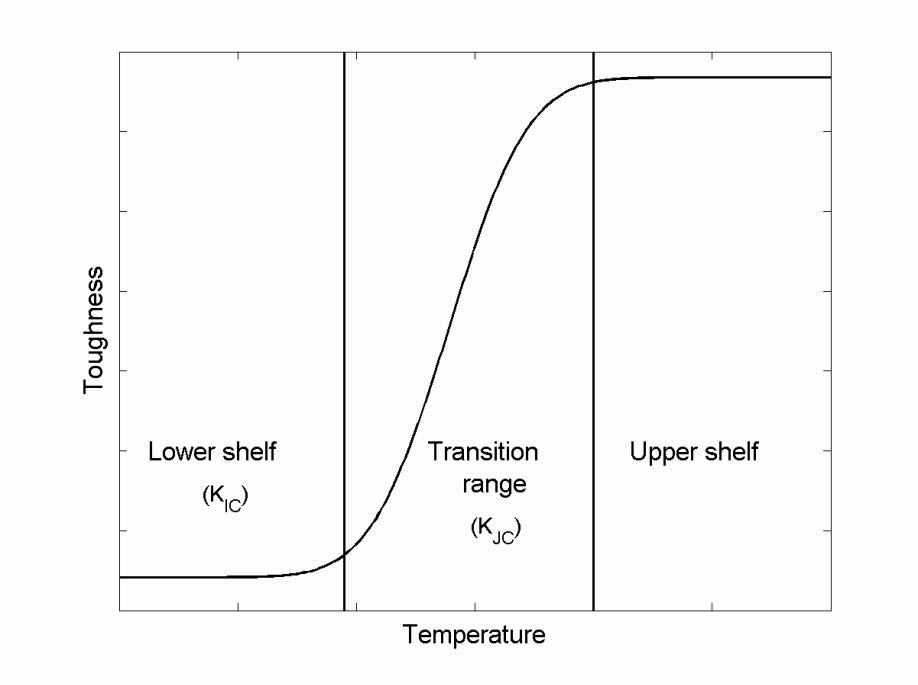

Fig. 13. Fracture mechanic characteristics for ferritic steels.

A method for evaluation of the fracture toughness results in the transition range and lower shelf regime has been presented by Wallin, called the master curve method [26]. This method has been adopted for ferritic steels in the American testing and analysis standard ASTM E1921-97 [84] and has been validated for a large number of materials. It has been shown experimentally for ferritic steels that the temperature dependence of the fracture toughness is only slightly material and yield strength dependent. The master curve method is developed by a statistical data treatment methodology and elastic plastic finite element analysis which makes it possible also to test small specimens in the ductile to brittle transition regime [85]. Bend specimens with a geometry down to 3 × 4 mm have been used successfully to determine the master curve. The fracture toughness results in the ductile to brittle transition regime have usually a large scatter and influence of the specimen size. This master curve method accounts for these effects as well as the temperature dependence of the fracture toughness [86].

$$K_{JC} = 20 + \left(11 + 77\exp\left[0.019\left(T - T_0\right)\right]\right) \times \left(\frac{25}{B}\right)^{0.25} \times \left(-\ln\left(1 - P_f\right)\right)^{0.25} \qquad (11)$$

where T is the testing temperature, T_0 the transition temperature corresponding to a median fracture toughness of 100 MPa√m, B the thickness of the specimen and P_f the cumulative failure probability. The transition temperature is in the lower part of the increasing transition region, close to the lower shelf, characterizing onset of cleavage fracture at elastic or elastic-plastic instability. An example of a master curve analysis of a low alloyed, high purity ferritic steel can be found in Fig. 14 [87].

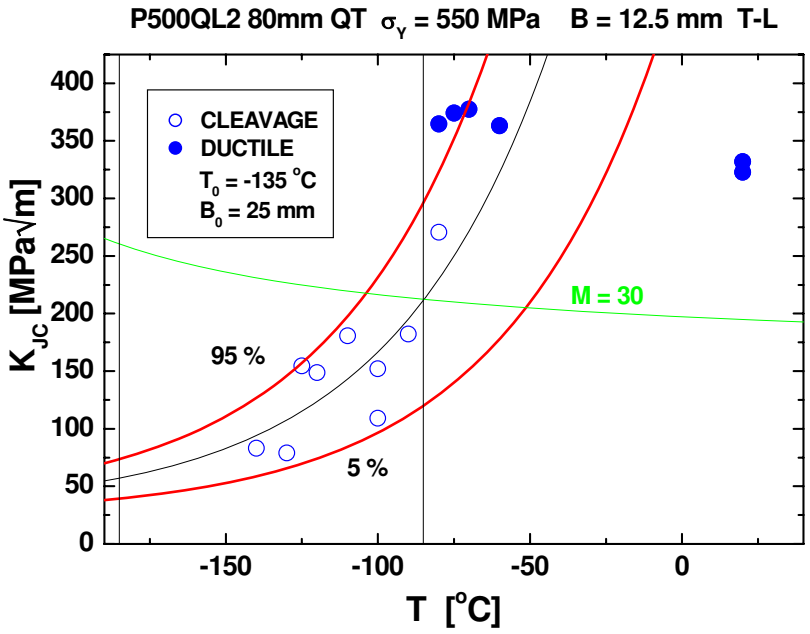

Fig. 14. Master curve analysis of a high strength quenched and tempered steel, P500QL2 [87].

The results from the highest testing temperatures are located at the upper shelf regime, see Fig. 13, which is not considered by the master curve analysis. Only data below the censoring limit are valid K_{JC} values.

$$K_{JC_{\lim it}} \le \sqrt{\frac{Eb\sigma_{ys}}{M\left(1-\nu^2\right)}} \qquad (12)$$

where E is the modulus of elasticity, b the distance between the crack tip and the back face of the specimen, σ_{ys} the yield strength, ν the Poisson ratio and M a size criterion constant. The master curve method applies an M value of 30. The censoring limit can be found in Fig. 14, designated as M=30.

The fracture behaviour of a material can be evaluated by impact or fracture toughness testing. These testing methods are rather different, fracture toughness testing using a deep crack and static loading rate, impact toughness testing using a short blunt notch and dynamic

loading. However, these differences oppose each other and the total effect is relatively small, in particular for high strength steels [88]. A high loading rate increases, while a blunt notch decreases the transition temperature. High strength steels offer low strain hardening and the influence from various loading conditions is consequently small. Fracture toughness testing is rather cost intensive and it is important to be able to correlate the impact and fracture toughness results, which has been done successfully by the following relation [88]:

$$T_0 = T_{28J} - 18 \qquad (13)$$

where T_{28J} is the transition temperature for an impact energy of 28 J and T_0 is the temperature where K_{JC} is 100 MPa√m. This correlation was verified by Wallin for 141 steels [88], with yield strengths between 300 and 1000 MPa. The relation is illustrated in Fig. 15 [88].

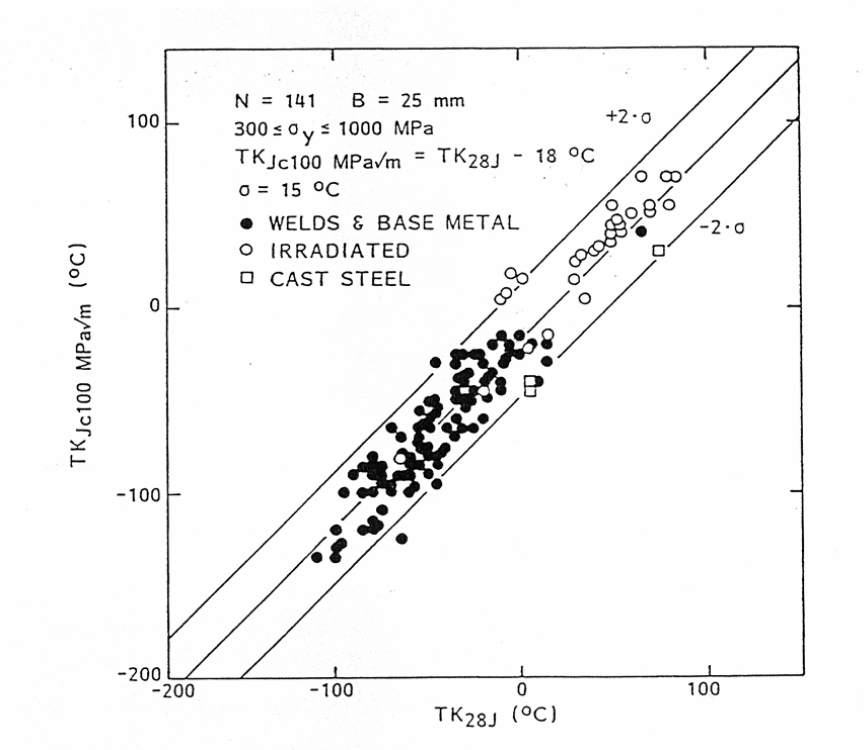

Fig. 15. Correlation between T_{28J} and T_0 [88].

4.1 Application of recent fracture mechanics findings

High and reliable toughness is of major concern in many applications. For safe design, fracture mechanics based codes are available, such as the code for steel structures, Eurocode 3 [89]. For pressure vessels, national codes based on fracture mechanics have been developed for design against brittle failure [90, 91]. The Swedish national code was used as a basis for the European pressure vessel standard, EN 13445, which allows the selection of steels up to a yield strength of 460 MPa and thickness of 110 mm [25]. The application of modern high

strength steels, such as DSS, is not yet fully covered within the code. Hence, expensive and time consuming fracture toughness testing has to be applied if these steels shall be utilised for pressure vessels. A number of new fracture mechanics tools have been developed recently [26-28] and a revision of EN 13445 is taking place in order to include high strength steels, such as DSS.

The modifications of the model include a scatter term of 100 MPa for the difference between the minimum and typical yield strength, instead of the previous scatter factor of 1.4. Moreover, plasticity changes the stress intensity and the residual stresses and these effects are also considered in the revision. The largest influence from the modifications comes from the thickness correction, which is based on the master curve approach by Wallin. The total effect on the minimum design temperature from these modifications are between -9 and -29 °C for the as-welded condition and between 5 and -15 °C for the post weld heat treated condition.

The model which was the basis for design against brittle failure in EN 13445 [24] assumes that an elliptical surface crack with a quarter thickness depth can be detected by non-destructive testing. However, this assumption is questionable for thinner gages where the cracks have to cover a larger fraction of the thickness to be safely observed. A relation between the maximum permissible crack depth and the thickness has been proposed [92, 93]. With this modification, the revised model values are even closer to the original code values.

The master curve method and the correlation between fracture and impact toughness were developed for ferritic steels, but the applicability to DSS also seems to be satisfactory. The development of the fracture mechanics model in EN 13445 have been summarised by Sandström et al [93, 94].

5. Fracture toughness testing in the thesis

Fracture mechanical testing has been performed in a test rig, specially developed for component testing (Fig. 16). The test rig is composed of three servo-hydraulic cylinders, individually managed by closed loop systems. Two of the cylinders have a capacity of 100 kN and one of 50 kN. The amplitude of the cylinders is +/- 75 mm. New customized hardware and software, controlling the loading condition, have been installed and a three point loading fixture has been developed, including a cooling box (Fig. 17) for low temperature testing. The box is filled with alcohol and contains chambers for liquid nitrogen. The alcohol is stirred and can be cooled down to approximately -110°C.

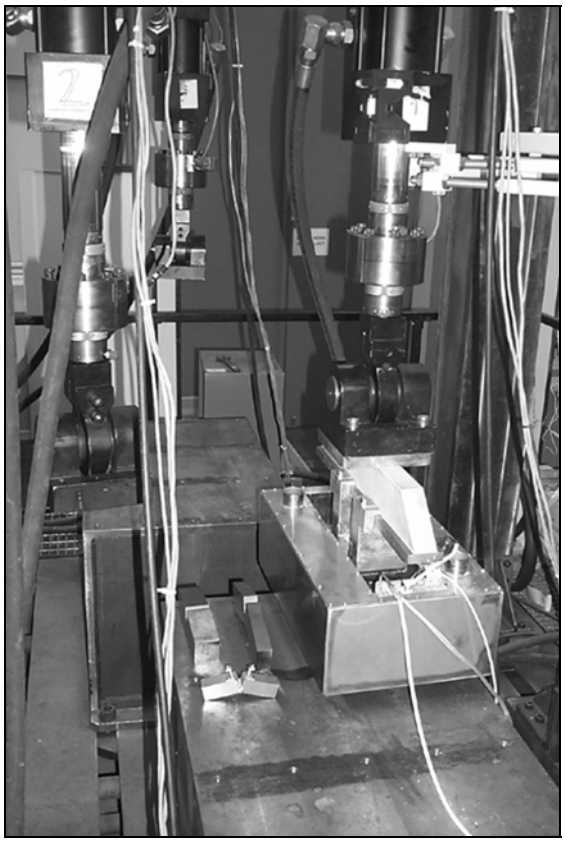

Fig. 16. Component test rig

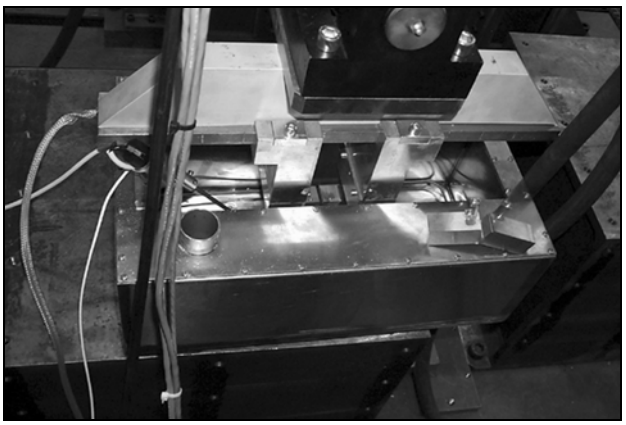

Fig. 17. Cooling box

The control system makes it possible to build up a system design with the customized conditions desired for varying types of tests. Displacement or load controlled testing for fatigue or static type can be managed with varying form of amplitude and strain rate. There is a great flexibility in how the motion/force can be supplied. Sinusoidal, triangle and square form of the fatigue curve can be supplied with varying amplitude during the same test. The test system design is built up by selecting movers to impart the desired forces/motions and by choosing transducers to monitor and control the test conditions. The mover and transducer choices are grouped together as needed and integrated into a mechanical design that introduces the movements appropriately. The control system subtracts the load cell feedback with the command signal to determine the error, which is processed to achieve the desired command value. The fracture toughness testing was carried out in accordance with ASTM E 1921-97 [84], with some modifications pointed out by Wallin [95]. This standard has been applied since it is based on the master curve approach, including calculations of a reference temperature which can be correlated to an impact toughness transition temperature, T_{28J}. Base and weld materials were tested and gave an estimation of the critical value of J, J_C, near the onset of stable crack extension, provided that the criteria concerning validity was fulfilled [84]. The test method is based on elasto-plastic theories and determination of a reference

temperature (T_0). The reference temperature corresponds to the temperature where the fracture toughness is 100 MPa√m, which characterizes the onset of cleavage cracking. The reference temperature is used to establish a transition temperature curve, the master curve.

The geometries of the specimens tested included 30×30, 30×60 and 50×50 mm. All specimens were full-thickness single-edge-notch bend-bars. A three point bend specimen can be found in Fig. 18.

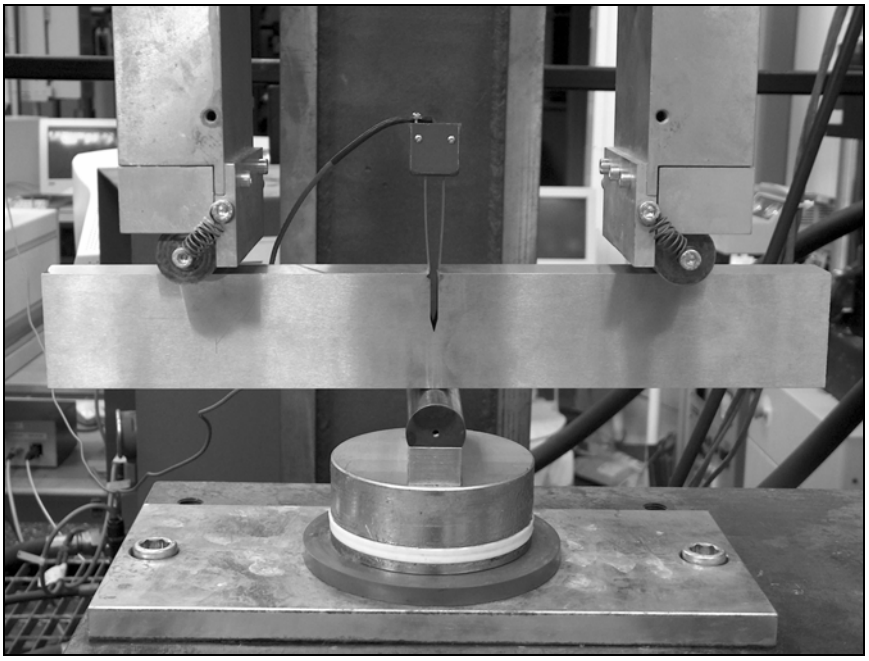

Fig. 18. Three point bend specimen (30×60×400 mm) and clip gauge, measuring the crack mouth opening displacement (CMOD).

The notches were machined transverse-longitude (T-L) and transverse-short (T-S) into the material (The T-L oriented notch is located in the transverse plane in the longitude direction, and the T-S oriented notch is located in the transverse plane in the short direction). After being prefatigued at room temperature to an initial crack length (notch + fatigue crack) of 50-60% of the width, the specimens were subjected to an increasing monotonic force. The loading rate was 0.1 mm/sec. Measurements were made of the force and the crack mouth opening displacement (CMOD) to the point at which either brittle crack extension occurs, a maximum force plateau is reached or a pop-in can be observed. Two different clip gauges measured the crack mouth opening displacement. The crack length during prefatigue was measured by an elastic compliance technique, where the force and crack mouth opening displacement are measured during elastic loading and unloading [96]. The specimens were side-grooved after precracking to achieve a straight crack front. The depth of each side-

groove was 10% of the thickness. Testing temperatures were selected between –40 and –112°C.

6. Contributed papers

Paper 1: Fracture toughness of a welded duplex stainless steel

The present work includes fracture toughness testing on 30 and 50 mm thick duplex stainless steel 2205 (22% Cr, 5.5% Ni, 3% Mo, 0.15% N). Base metal and submerged arc weldments (SAW) at subzero temperatures have been tested using full size three point bending. The evaluation of the results has been carried out using J-integral calculations and correlations to impact toughness. It is shown that the temperature dependence of the fracture can be described by a transition temperature curve, the master curve. A reference temperature, T_0, where the fracture toughness is 100 MPa√m has been determined. In addition, crack tip opening displacement (CTOD) has been calculated for comparison with earlier investigations. Microstructure studies showed a fine elongated lamellar structure in the base material and coarse columnar grains in the weld material. A varying amount of dimple rupture was found in both base and weld metal. The present study shows that the duplex stainless steel 2205 has high fracture toughness. The reference temperature was -143°C for the base material and -101°C for the weld material, see Fig. 19.

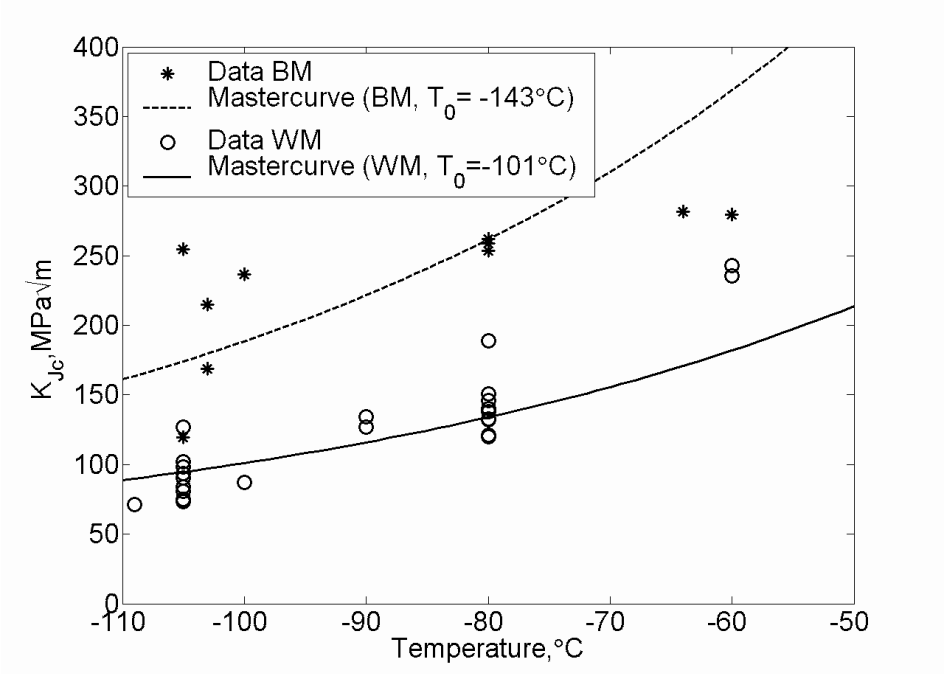

Fig. 19. Fracture toughness of base and weld material of duplex stainless steel 2205.

Paper 2: Fracture toughness of the lean duplex stainless steel LDX 2101

Fracture toughness testing has been performed on the recently developed lean duplex stainless steel LDX 2101 (EN 1.4162, UNS S32101). The results were evaluated by the master curve analysis, including deriving a reference temperature. The master curve approach, originally developed for ferritic steels, has been used successfully. The reference temperature corresponds to a fracture toughness (K_{JC}) of 100 MPa√m, which characterizes onset of cleavage cracking at elastic and/or elastic-plastic instabilities. The reference temperature, T_0, was -112 °C and -92 °C for the base and weld material, respectively. In addition, crack tip opening displacements have been calculated as well as comparisons between fracture and impact toughness results. Good toughness properties have been found in traditional duplex stainless steels, while the present study has verified high fracture toughness also for a low alloyed grade. The fracture toughness was somewhat lower than for 2205 (EN 1.4462), but still quite satisfactory for both base and weld material even for many low temperature applications. The evaluated K_{JC} values together with the master curves for the base and weld material testing can be found in Fig. 20.

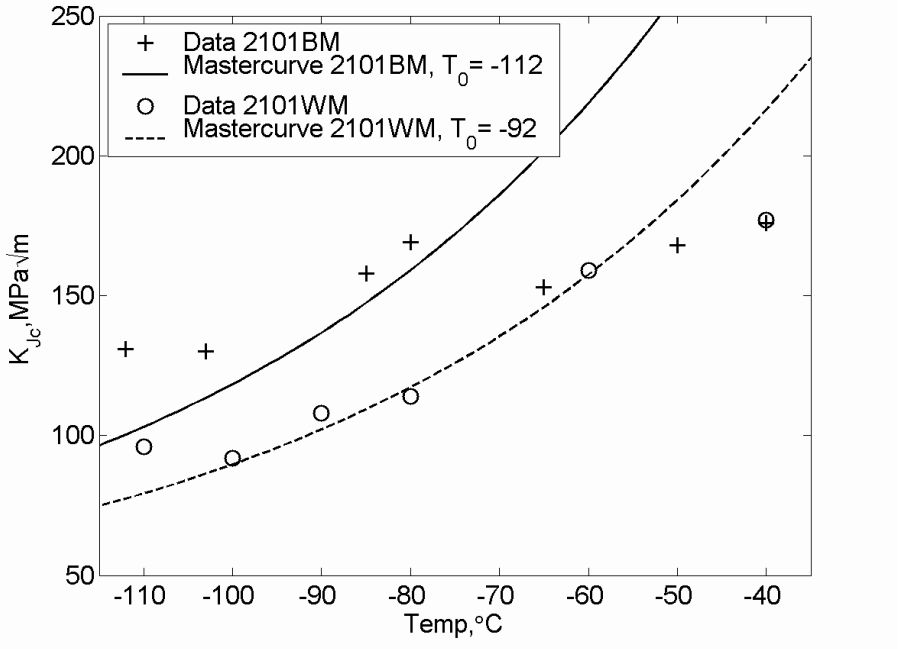

Fig. 20. K_{JC} data and corresponding master curves for LDX 2101 base and weld material.

Paper 3: Crack detection performance and other assumptions for implementation in a model for avoidance of brittle fracture in pressure vessel steels

A model in the European pressure vessel standard EN 13445 for prevention of brittle failure has been analysed using recent fracture mechanical results from ECOPRESS, SINTAP, and other recent European research projects. Although it is recommended that some basic parts of the model are exchanged, practically all of the output of the model is consistent with more recent findings. The main concern involves the crack detection. A maximum allowed crack depth of 25 % of the thickness is assumed in EN 13445, which is now believed to be too optimistic for thin gauges. This fraction is proposed to decrease with the thickness. To characterise the crack detection performance, a parameter (t_{50}) is introduced for the thickness where a crack with a depth of half the specimen thickness can readily be detected.

An expression of the maximum tolerable crack depth (a) as a function of the gauge thickness (t) is proposed

$$a = \Theta(t)t \tag{14}$$

where

$$\Theta(t) = 1 - \frac{3}{4}\tanh\left(\frac{t}{t_0}\right) \tag{15}$$

Analysis of literature on non-destructive testing techniques indicates that t_{50}=15 mm, i.e. t_0=18.6, gives a sufficiently safe design model, see Fig. 21.

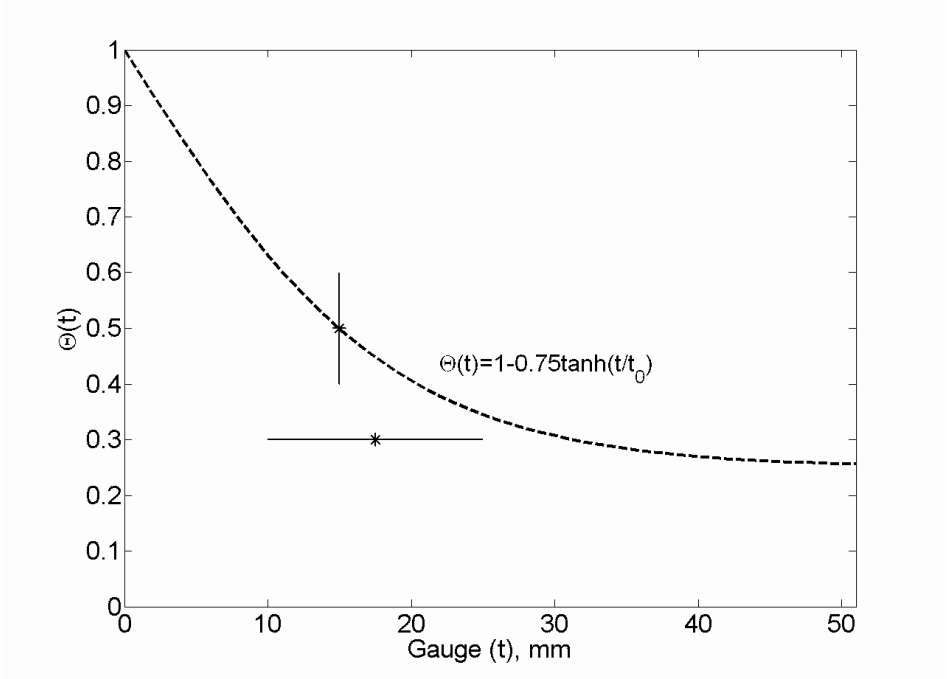

Fig. 21. The influence of the gauge thickness (t) on the function Θ(t). Results from two different projects are added to the figure.

Paper 4: Austenite reformation in the heat-affected zone of duplex stainless steel 2205

The aim of the present work has been to evaluate the amount of reformed austenite in the heat affected zone (HAZ) of submerged arc welded (SAW) duplex stainless steel 2205. The model is based on calculations of the nucleation and growth of austenite, controlled by nitrogen diffusion. Two existing heat flow models have been used to predict the cooling time. The results have been compared successfully with microstructure studies and literature data. The results indicate that cooling the weld in air provides a satisfactory amount of reformed austenite, see Fig. 22.

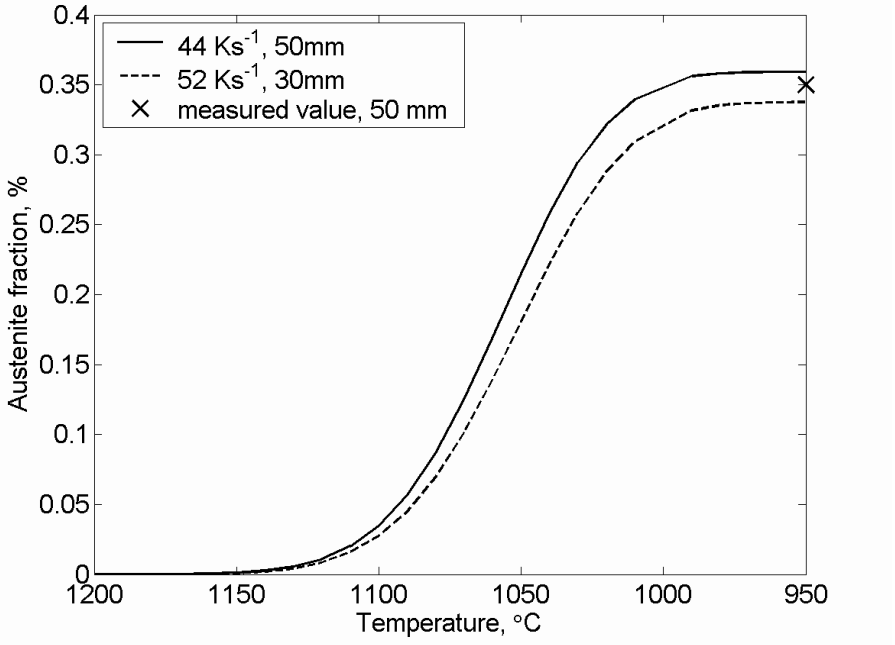

Fig. 22. Comparison of austenite reformation for different cooling rates.

Paper 5: Sigma precipitation in duplex stainless steel 2205

Sigma phase precipitation is known to embrittle duplex stainless steel. Accordingly, heat treatment and welding must be performed carefully. Nucleation and diffusional growth of sigma phase in the duplex stainless steel 2205 have been evaluated in order to ensure the high toughness shown in previous studies for both base and weld material. The model gives a satisfactory estimation of sigma phase precipitated both during isothermal aging and continuous cooling. Isothermal results of the present model are compared with experimental references in Fig. 23. The present model shows TTT-curves for 1, 3, 5 and 10% sigma precipitation.

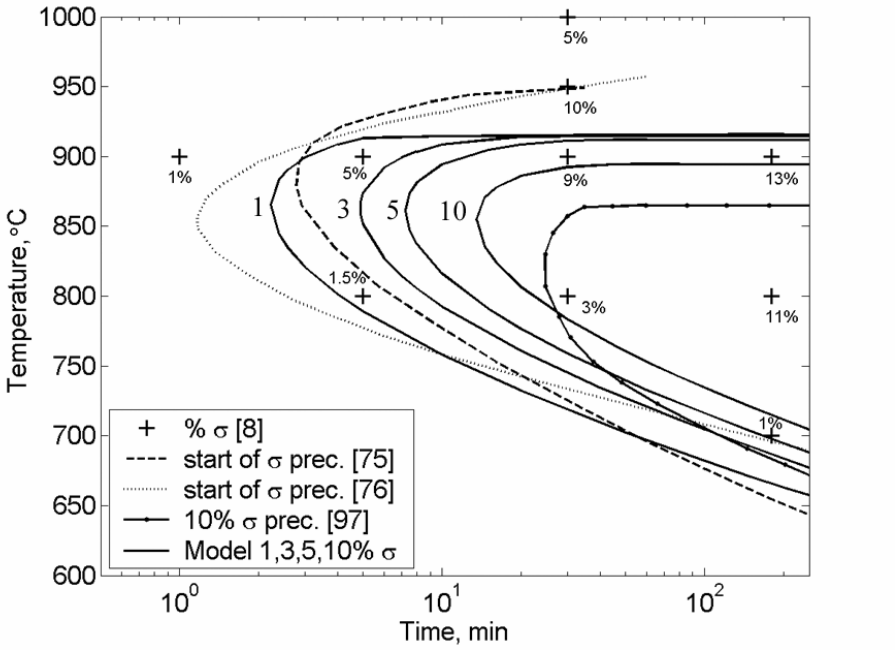

Fig. 23. Isothermal sigma precipitation by present model and literature references.

Paper 6: Modelling solid solution hardening in stainless steels

The solid solution hardening of stainless steels has been studied by using the Labusch-Nabarro relation. Models have been evaluated in order to predict the mechanical properties from chemical composition, solution hardening misfit parameters, grain size, ferrite content and product thickness. A data source of six grades of steels has been used for the modelling. Both austenitic and duplex stainless steels have been covered including more than 1100 batches, which have been applied to multiple regression analyses. The models are compared with earlier studies and can be used as tools in material optimisation. Regression analysis of tensile strength data, together with literature references, can be found in Fig. 24.

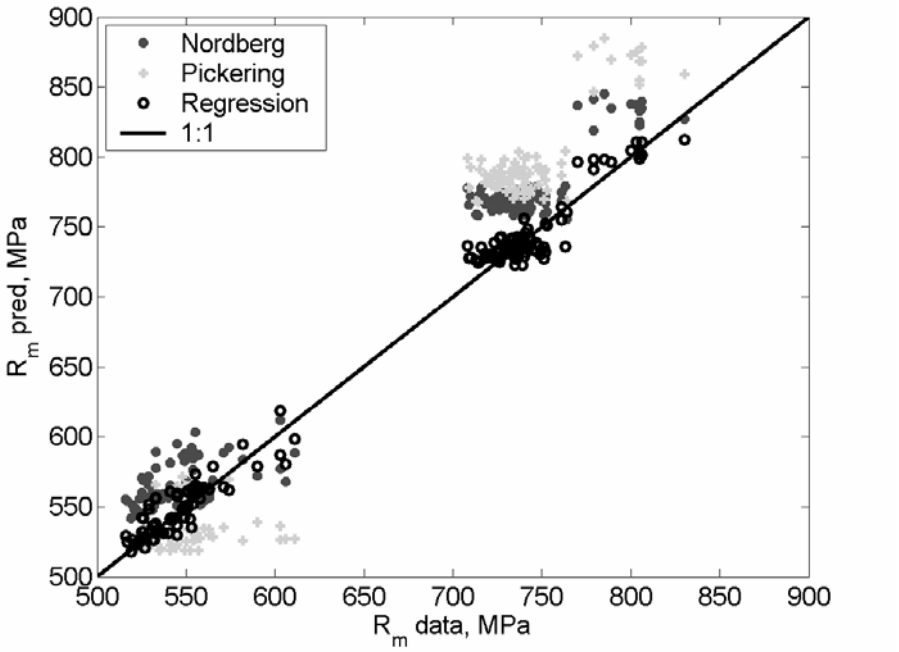

Fig. 24. Measured tensile strength (room temperature) compared with tensile strength evaluated by the present multiple regression analysis and with models of Pickering and Nordberg. The amount data was randomly reduced from 1114 to 150 data points to improve visibility.

7. Conclusions

Fracture mechanical testing has verified high fracture toughness in both the base and the weld material of DSS 2205, reference temperatures -143/-101^{0}C, and LDX 2101, reference temperatures -112/-92^{0}C. The reference temperature corresponds to the temperature at which the fracture toughness is 100 MPa√m, which characterizes the onset of cleavage cracking. The master curve method, originally developed for ferritic steels, was used successfully for evaluation of the results.

Some basic assumptions in a modified brittle fracture model intended for use in EN 13445 have been presented. The model uses a minimum crack size, which will always be found during modern non-destructive testing (NDT). It is shown that a crack depth of a quarter thickness can be applied at thick gauges. For thinner gauges, a function describing the minimum detectable crack depth can be used, which gradually goes to full thickness when the gauge thickness decreases. A relation between the minimum detectable crack depth and the specimen thickness is proposed, based on a parameter (t_{50}), describing the minimum thickness where a crack penetrating half the specimen thickness can be detected. A t_{50} value of 15 mm is proposed.

The austenite reformation in the HAZ of DSS 2205 has been modelled by calculations of the nucleation and diffusion controlled growth. Two established methods were used to predict the cooling time. The model for austenite reformation was also used, with some modifications, to evaluate the sigma precipitation during heat treatment and cooling. The predicted austenite and sigma phase fractions agree well with microstructure analysis and with literature references. Cooling DSS (2205) weldments (SAW) in air using present welding parameters provides a satisfactory phase balance and avoidance of brittle intermetallic precipitates.

The solid solution hardening in stainless steels has been studied to find approximate relations between mechanical properties and the chemical composition, grain size, ferrite content and product thickness. The solution hardening effect was successfully predicted by the Labusch-Nabarro relation and multiple regression analyses were used to evaluate hardening equations for stainless steels. The results of the regressions are satisfactory for strength and ductility with good statistical significance. For future stainless steel development, the availability of satisfactory correlations between composition, microstructure and mechanical properties are essential to optimise alloy compositions in the development of new stainless steels.

8. Acknowledgments

This thesis was financially supported by the EU Growth project EcoPress, Outokumpu Stainless, Sandvik Materials Technology and the Brinell centre at KTH. Outokumpu Stainless and Sandvik Materials Technology are gratefully acknowledged for supplying materials and performing welding. I also wish to thank the following persons:

- My supervisor Professor Rolf Sandström, who made it possible for me to write this thesis. I wish to express my sincere gratitude for his patient support and excellent guidance.
- Partners within the EcoPress project for the allowance of the use of results prior to publication.
- Elin Westin at Outokumpu Stainless and Guocai Chai at Sandvik Materials Technology for supplying me with test specimens and for answering all my material and weld related questions.
- My colleagues at the department of Materials Science and Engineering and at the division of Materials Technology for enjoying lunches and discussions.
- Dennis Andersson for his general knowledge and all-embracing assistance.
- Günther Nabholz at SweTest AB for design, manufacturing and service of the test-rig.
- P.O Söderholm and Hans Bergkvist for microscope support.
- My family and friends.
- Josse.

9. References

1. Duplex stainless steel, Outokumpu, http://www.outokumpu.com/29153.epibrw.
2. Vogt J.-B., Fatigue properties of high nitrogen steels, Mater. Proc. Tech., 117 (2001) 364-369.
3. Mateo A., Llanes L., Akdut N., Anglada M., High cycle fatigue behaviour of a standard duplex stainless steel plate and bar, Mater. Sci. Eng. A, 319-321 (2001) 516-520.
4. Charles J., Composition and properties of duplex stainless steels, Weld. World (UK), 36 (1995) 43-54.
5. Nilsson J.-O., Super duplex stainless steels, Mater. Sci. Tech., 8 (1992) 685-700.
6. Thorvaldsson T., Eriksson H., Kutka J., Salwén A., Influence of microstructure on mechanical properties of a duplex stainless steel, Stainless Steel ‘84, Göteborg, Sweden, 1 (1984) 101-105.
7. Gunn R. N., Reduction in fracture toughness due to intermetallic precipitates in duplex stainless steels, Duplex America 2000, Houston, USA, (2000) 299-314.

8. Karlsson L., Bengtsson L., Rolander U., Pak S, The kinetics of intermetallic phase formation in duplex stainless weld metals and their influence on mechanical properties, Applications of Stainless Steel '92, Stockholm, Sweden, 1 (1992) 335-344.
9. Hertzman S., Lehtinen B., Symniotis-Barradal E., Intermetallic phase formation and its effect on corrosion resistance of duplex stainless steel SS 2377 (UNS 31803), Applications of Stainless Steel '92, Stockholm, Sweden, 1 (1992) 345-359.
10. Karlsson L., Rigdal S., Lake F., Effects of intermetallic phases in duplex stainless steel weldments, Duplex America 2000, Houston, USA, (2000) 257-272.
11. Karlsson L., Duplex stainless steel weld metals-effects of secondary phases, Duplex Stainless Steels ’97, Maastricht, Netherlands, 1 (1997) 43-58.
12. Liljas M., The welding metallurgy of duplex stainless steels, Duplex Stainless steels ´94, Glasgow, Scotland, 1994.
13. McPherson N. A., Chi K., Baker T. N., Submerged arc welding of stainless steel and the challenge from laser welding process, J. Mater. Proc. Tech., 134 (2003) 174-179.
14. Van Nassau L., Meelker H., Hilkes J., Welding duplex and super-duplex stainless steels, Duplex Stainless Steels '91, Beaune, France, 1 (1991) 303-323.
15. Nicodemi W., Roberti R., La Wecchia G. M., Duplex Stainless Steel Microstructure and Toughness, Applications of Stainless Steel '92, Stockholm, Sweden, 1 (1992) 270-279.
16. Nyström M., Karlsson B., Wasén J., The Mechanical Properties of a Duplex Stainless Steel, Nordic Symposium on Mechanical Properties of Stainless Steels, Sigtuna, Sweden, (1990) 70-87.
17. Charles J., Why and where duplex stainless steels, Duplex Stainless Steels ’97, Maastricht, Netherlands, 1 (1997) 29-42.
18. Deleu E., Dhooge A., Fracture toughness of welded thick walled duplex stainless steels, , Duplex Stainless Steels ’97, Maastricht, Netherlands, 1 (1997) 387-394.
19. Dhooge A., Deleu E., Low temperature fracture toughness of thick duplex and superduplex stainless steel weldments, Weld. World (UK), 39 (1997) 47-52.
20. Johansson R. E., Nilsson J.-O., Fracture Toughness of Austenitic and Duplex Stainless, Stainless Steel '84, Göteborg, Sweden, (1984) 446-451.
21. Ericsson C., Sandström R., Sieurin H., Lagerqvist O., Eisele U., Sciedermaier J., Ruiz R. L., Background document 3.5, EcoPress, European research 5th framework, 2003.
22. Johansson P., Liljas M., A new lean duplex stainless steel for construction purposes, ACOM, Sweden, 1-2 (2002) 17-23.
23. Sanz G., Attempts to introduce a quantitative method of choosing steel quality with reference to the risk of brittle fracture, Rev. Metall. CIT, 77 (1980) 621-642.
24. Sandström R., Minimum usage temperature for ferritic steels, Scand. J. Metall., 16 (1987) 242-252.
25. EN 13445-2, Unfired pressure vessels—part 2—materials, CEN, Brussels (2002).
26. Wallin K., The master curve method: a new concept for brittle fracture, Int. J. Mat. Prod. Tech., 14 (1999) 342-354.
27. Structural Integrity Assesment Procedure (SINTAP), Final Revision, EU-project BE95-1462, Brite-Euram programme (1999).

28. Milne I., Ainsworth R. A., Dowling A. R., Stewart A. T., Background to and validation of CEGB Report R/H/R6--Revision 3, Int. J. Pres. Ves. Pip., 32 (1998) 105-196.
29. Langenberg P., Edit. ECOPRESS, Economical and safe design of pressure vessels applying new modern steels, European research project, 5th framework RTD, project no. GRD1-1999-10640, 1/2000-5/2003, Final Report, (2003).
30. Brinell centre, MATOP, http://www.brinell.kth.se/MatOp/index.htm.
31. Stainless steel world, High performance stainless steels, http://www.stainless-steel-world.net/pdf/11021.pdf.
32. Nilsson J.-O., Kangas P., Karlsson T., Wilson A., Microstructural stability and mechanical properties of a high nitrogen super duplex stainless steel, Mater. Sci. Forum, 318-320 (1999) 751-756.
33. Nilsson J.-O., Kangas P., Karlsson T., Wilson A., Mechanical properties, microstructural stability and kinetics of σ-phase formation in 29Cr-6Ni-2Mo-0.38N superduplex stainless steel, , Metall. Mater. Trans. A, 31A (2000) 35-45.
34. Stainless steel world, Duplex stainless steel grades, http://www.stainless-steel-world.net/duplex/grades.asp.
35. Sandvik SAFUREX, Material datasheet S-1847, Sandvik, 2004.
36. Super duplex stainless steel defies caustic soda corrosion, Adv. Mater. Proc., 161 (2003) 7-8.
37. DeLong W. T., Ferrite in austenitic stainless steel weld metals, Weld. J., 53 (1974) 273-286.
38. Welding consumables, http://www.avestawelding.com.
39. Steel grades, properties and global standards, http://www.outokumpu.com
40. Smuk O., Microstructure and properties of modern P/M super duplex stainless steels, PhD. Thesis, Dept. Mater. Sci., KTH, Stockholm, Sweden, 2004.
41. Charles J., Super duplex stainless steels: Structure and properties, Duplex Stainless Steels ’91, Beaune, France, 2 (1991) 3-48.
42. Park Y.-H., Lee Z.-H., The effect of nitrogen and heat treatment on the microstructure and tensile properties of 25Cr-7Ni-1.5Mo-3W-xN duplex stainless steel castings, Mater. Sci. Eng. A, 297 (2001) 78-84.
43. Nordberg H., Mechanical properties of austenitic and duplex stainless steels, La Metall. Ita., 85 (1994) 147-154.
44. Sieurin H., Zander J., Sandström R., Modelling solid solution hardening in stainless steels, Mater. Sci. Eng. A, 415 (2006) 66-71.
45. Benson M., Applications utilising the advantageous properties of LDX 2101 (EN 1.4162, UNS S32101), stainless steel world 2005, P5038.
46. Iacoviello F., Boniardi M., La Vecchia, G. M., Fatigue crack propagation in austeno-ferritic duplex stainless steel 22 Cr 5 Ni, Int. J. Fatigue, 21 (1999) 957-963.
47. Stolarz J., Foct J., Specific features of two phase alloys response to cyclic deformation, Mater. Sci. Eng. A, 319-321 (2001) 501-505.
48. Vogt J.-B., Massol K., Foct J., Role of the microstructure on fatigue properties of 475 °C aged duplex stainless steels, Int. J. Fatigue, 24 (2002) 627-633.

49. Ekström U., Olsson K., The influence of ferrite and oxygen contents on weld metal mechanical properties of submerged-arc welded stainless steels, Weld pool chemistry and metallurgy, London, UK, (1980) 323-334.
50. Fourlaris G., Maylin M. G., Gladman T., A comparative study of the mechanical, magnetic and microstructural characteristics of modified SAF 2205 and 2507 type duplex austenitic-ferritic stainless steels, Mater. Sci. Forum, 318-320 (1999) 805-810.
51. Gough P. C., Farrar J. C. M., Fracture toughness of duplex and superduplex stainless steel welds, Duplex Stainless Steels ’97, Maastricht, Netherlands, 1 (1997) 483-490.
52. Weman K., Welding processes handbook, ESAB, 2002.
53. Lippold J. C., Lin W., Brandi S., Varol I., Baeslack W. A., Heat-affected zone microstructure and properties in commercial duplex stainless steels, Duplex Stainless steels ´94, Glasgow, Scotland, 1994.
54. Hertzman S., Roberts W., Lindenmo M., Microstructure and properties of nitrogen alloyed stainless steel after welding treatments, Duplex Stainless steels ´86, Netherlands, Hague, (1986) 257-263.
55. Hoffmeister H., Lothongkum G., Quantitative effects of nitrogen contents and cooling cycles on δ-γ transformation, chromium nitride precipitation and pitting corrosion after weld simulation of duplex stainless steels, Duplex Stainless steels ´94, Glasgow, Scotland, 2 (1994) .
56. Ahn S. K., Choi D. Y., Lee S. C., Lee Y. D., Impact properties and susceptibility to solidification cracking of the weld in 22 Cr duplex stainless steel, Duplex Stainless Steels ’97, Maastricht, Netherlands, 1 (1997) 357-367.
57. Hertzman S., The influence of nitrogen on microstructure and properties of highly alloyed stainless steel welds, ISIJ Int., 41 (2001) 580-589.
58. Cao H.-L, Hertzman S., The relationship between impact properties and welding simulated microstructures in three duplex stainless steels, Duplex Stainless Steels '91, Beaune, France, 1 (1991) 363-372.
59. Charles J., Structure and mechanical properties of duplex stainless steels, Duplex Stainless steels ´94, Glasgow, Scotland, 1994.
60. Muthupandi V., Bala Srinivasan P., Seshadri S. K., Sundaresan S., Effect of weld metal chemistry and heat input on the structure and properties of duplex stainless steel welds, Mater. Sci. Eng. A, 358 (2003) 1-8.
61. Sato Y. S., Nelson T. W., Sterling C. J., Steel R. J., Pettersson C.-O., Microstructure and mechanical properties of friction stir welded SAF 2507 super duplex stainless steel, Mater. Sci. Eng. A, 397 (2005) 376-384.
62. Dijkstra F. H., de Raad J. A., Non-destructive testing of duplex welds, Duplex Stainless Steels ’97, Maastricht, Netherlands, 1 (1997) 509-517.
63. Cortie M. B., Jackson E. M. L. E. M., Simulation of the precipitation of sigma phase in duplex stainless steels, Metall. Mater. Trans. A, 28 (1997) 2477-2484.
64. Sundman B., Jansson B., Andersson J.-O., The Thermo-Calc Databank System, CALPHAD, 9 (1985) 153-190.

65. Redjaimia A., Metauer G., Gantois M., Decomposition of delta ferrite in a Fe-22Cr-5Ni-3Mo-0.03C Duplex stainless steel. A morphological and structural study, Duplex Stainless Steels ’91, Beaune, France, 1 (1991) 119-126.
66. Chen T. H., Yang J. R., Microstructural characterization of simulated heat affected zone in a nitrogen-containing 2205 duplex stainless steel, Mater. Sci. Eng. A., 338 (2002) 166-181.
67. Atamert S., King J. E., Intragranular nucleation of austenite, Zeitschrift fur Metallkunde, 82 (1991) 230-239.
68. Hertzman S., Ferreira P. J., Brolund B., An experimental and theoretical study of heat-affected zone austenite reformation in three duplex stainless steels, Metall. Mater. Trans. A, 28A (1997) 277-285.
69. Muthupandi V., Bala Srinivasan P., Shankar V., Seshadri S. K., Sundaresan S., Effect of nickel and nitrogen addition on the microstructure and mechanical properties of power beam processed duplex stainless steel (UNS 31803) weld metals, Mater. Lett., 59 (2005) 2305-2309.
70. Atamert S., King J. E., Super duplex stainless steels. Part 1. Heat affected zone microstructures, Mater. Sci. Techn, 8 (1992) 896-911.
71. Josefsson B., Nilsson J.-O., Wilson A., Phase transformations in duplex steels and the relation between continuous cooling and isothermal heat treatment, Duplex Stainless Steels '91, Beaune, France, 1 (1991) 67-78.
72. Chen T. H., Yang J. R., Effects of solution treatment and continuous cooling on σ-phase precipitation in a 2205 duplex stainless steel, Mater. Sci. Eng. A, 311 (2001) 28-41.
73. Huang C.-S., Shih C.-C., Effects of nitrogen and high temperature aging on σ-phase precipitation of duplex stainless steel, Mater. Sci. Eng. A, 402 (2005) 66-75.
74. Duprez L., De Cooman B. C., Akdut N., Redistribution of the substitutional elements during σ and χ phase formation in a duplex stainless steel, Steel research, 72 (2001) 311-316.
75. Li X., Miodownik A. P., Saunders N., Modelling of materials properties in duplex stainless steels, Mater. Sci. Technol., 18 (2002) 861-868.
76. Duprez L., De Cooman B. C., Akdut N., Microstructural changes in duplex stainless steel during isothermal annealing, 6th World Duplex Conference & Expo, Venice, Italy, (2000) 355-365.
77. Chen T. H., Weng K. L., Yang J. R, The effect of high-temperature exposure on the microstructural stability and toughness property in a 2205 duplex stainless steel, Mater. Sci. Eng. A, 338 (2002) 259-270.
78. Nilsson J.-O., Wilson B., Josefsson B., Thorvaldsson T., Relationship between pitting corrosion, toughness and microstructure for isothermally heat treated super duplex stainless steel, Applications of Stainless Steel '92, Stockholm, Sweden, 1 (1992) 280-289.
79. Lee K. M., Cho H. S., Choi D. C., Effect of isothermal treatment of SAF 2205 duplex stainless steel on migration of δ/γ interface boundary and growth of austenite, J. Alloys Comp., 285 (1999) 156-161.
80. El Koussy M. R., El Mahallawi I. S., Khalifa W., Al Dawood M. M., Bueckins M., Effects of thermal aging on microstructure and mechanical properties of duplex stainless steel, Mater. Sci. Techn, 20 (2004) 375-381.
81. ASTM E 399-99, Standard test method for plain-strain fracture toughness of metallic materials, Annual Book of ASTM Standards. vol. 03.01.

82. BS 7448, Fracture mechanics toughness tests, Method for determination of K_{Ic}, critical CTOD and critical J values of metallic materials, British Standard, Part 1.
83. BS 7448, Fracture mechanics toughness tests, Method for determination of K_{Ic}, critical CTOD and critical J values of welds in metallic materials, British Standard, Part 2.
84. ASTM E 1921-97, Standard test method for determination of reference temperature, T_0, for ferritic steels in the transition range, Annual Book of ASTM Standards. vol. 03.01.
85. Wallin K., Planman T., Valo M., Rintamaa R., Applicability of miniature size bend specimens to determine the master curve reference temperature T_0, Eng. Fract. Mech., 68 (2001) 1265-1296.
86. Pisarski H. G., Wallin K., The SINTAP fracture toughness estimation procedure, Eng. Fract. Mech., 67 (2000) 613-624.
87. Wallin K., Statistical test data analysis, background document 4, EcoPress, European research 5th framework, 2003.
88. Wallin K., Methodology for selecting Charpy toughness criteria for thin high strength steels. Jernkontorets forskning, report from working group 4013/89, 1990.
89. EUROCODE 3, Design of steel structures (part 1) pr ENV 1993-1. 1998 and design of steel bridges pr ENV 1993-2; 1999.
90. CODAP: French Code for the construction of unfired pressure vessels. Part M. Appendix MAZ; 1984.
91. Swedish pressure vessel code. Stockholm: Swedish pressure vessel commission: 1987.
92. Sieurin H., Sandström R, Langenberg P., Crack detection performance and other assumptions for implementation in a model for avoidance of brittle fracture in pressure vessel steels, 29th MPa Seminar, Stuttgart, Oct 9-10, 2003.
93. Sandström R., Langenberg P., Sieurin H., New brittle fracture model for the European pressure vessel standard, Int. J. Pres. Ves. Pip., 81 (2004) 837-845.
94. Sandström R., Langenberg P., Sieurin H., Analysis of the brittle fracture avoidance model for pressure vessels in European standard, Int. J. Pres. Ves. Pip., 82 (2005) 872-881.
95. Wallin K., Master curve analysis of the “Euro” fracture toughness dataset, Eng. Fract. Mech., 69 (2002) 451-481.
96. ASTM E 813-89, Standard test method for J_{IC}, a measure of fracture toughness, Annual Book of ASTM Standards. vol. 03.01.
97. Ahn Y. S., Kang J.P., Effect of aging treatments on microstructure and impact properties of tungsten substituted 2205 duplex stainless steel, Mater. Sci. Techn., 16 (2000) 382-388.